

# 1 **Technical Note: Lessons from and best practices for the** 2 **deployment of the Soil Water Isotope Storage System**

3 Rachel E. Havranek<sup>1</sup>, Kathryn Snell<sup>1</sup>, Sebastian Kopf<sup>1</sup>, Brett Davidheiser-Kroll<sup>2</sup>, Valerie Morris<sup>3</sup>, Bruce  
4 Vaughn<sup>3</sup>

5 Rachel Havranek, Kathryn Snell, Sebastian Kopf, Brett Davidheiser-Kroll, Valerie Morris, Bruce Vaughn

6 <sup>1</sup>Geological Sciences, University of Colorado Boulder, Boulder, 80303, USA

7 <sup>2</sup>Thermo Fisher Scientific (Bremen) GmbH, Bremen, Germany

8 <sup>3</sup>Institute of Arctic and Alpine Research, University of Colorado Boulder, Boulder, 80303, USA

9 *Correspondence to:* Rachel Havranek (rachel.havranek@colorado.edu)

10 **Abstract.** Soil water isotope datasets are useful for understanding connections between the  
11 hydrosphere, atmosphere, biosphere, and geosphere. However, they have been underproduced  
12 because of technical challenges associated with collecting those datasets. Here, we present the  
13 results of testing and automation of the Soil Water Isotope Storage System (SWISS). The unique  
14 innovation of the SWISS is that we are able to automatically collect water vapor from the critical  
15 zone at a regular time interval and then store that water vapor until it can be measured back in a  
16 laboratory setting. Through a series of quality assurance and quality control tests, we tested that  
17 the SWISS is resistant to both atmospheric intrusion and leaking in both laboratory and field  
18 settings. We assessed the accuracy and precision of the SWISS through a series of experiments  
19 where water vapor of known composition was introduced into the flasks, stored for 14 days, and  
20 then measured. From these experiments, after applying an offset correction to report our values  
21 relative to VSMOW, we assess the precision of the SWISS at  $\pm 0.9\text{‰}$  and  $\pm 3.7\text{‰}$  for  $\delta^{18}\text{O}$  and  
22  $\delta^2\text{H}$ , respectively. We deployed three SWISS units to three different field sites to demonstrate  
23 that the SWISS stores water vapor reliably enough that we are able to differentiate dynamics  
24 both between the sites as well within a single soil column. Overall, we demonstrate that the  
25 SWISS retains the stable isotope composition of soil water vapor for long enough to allow  
26 researchers to address a wide range of ecohydrologic questions.

## 27 **1 Introduction**

28 Understanding soil water dynamics across a range of environments and soil properties is  
29 critical to food and water security (e.g. Mahindawansa et al., 2018; Quade et al., 2019; Rothfuss  
30 et al., 2021); understanding biogeochemical cycles, such as the nitrogen and phosphorus cycles  
31 (e.g. Hinckley et al., 2014; Harms and Ludwig, 2016); and understanding connections between  
32 the hydrosphere, biosphere, geosphere and atmosphere (e.g. Vereeken et al., 2022). One  
33 approach that can be used to understand water use and movement in the critical zone is the stable  
34 isotope geochemistry of soil water (e.g. Sprenger et al., 2016; Bowen et al., 2019). Variations in  
35 the stable isotope ratios of oxygen and hydrogen of soil water ( $\delta^{18}\text{O}$ ,  $\delta^2\text{H}$ ) track physical  
36 processes like infiltration, root water uptake and evaporation. In particular, stable water isotopes  
37 are useful for disentangling complex mixtures of water from multiple sources (e.g. Dawson and  
38 Ehleringer, 1991; Brooks et al., 2010; Soderberg et al., 2012; Good et al., 2015; Bowen et al.,  
39 2018; Gomez-Navarro et al., 2019; Sprenger and Allen 2020). Despite the long-recognized  
40 utility of measuring soil water isotopes for understanding a range of processes (e.g. Zimmerman

41 et al., 1966; Peterson & Fry., 1987), soil water isotope datasets have been under-produced as  
42 compared to groundwater and meteoric water isotope datasets (Bowen et al., 2019).

43 The primary barrier to producing soil water isotope datasets has been the arduous nature  
44 of collecting samples. Historically, there are two primary methods for collecting soil water  
45 samples: either digging a pit and collecting a mass of soil to bring back to the lab for subsequent  
46 water extraction or via lysimeter. The former method disrupts the soil profile each time a sample  
47 is collected, inhibiting the creation of long-term records of soil water isotopes. Lysimeters on the  
48 other hand provide the means to collect multi-year soil water isotope datasets (e.g. Green et al.,  
49 2015; Groh et al., 2018; Hinkley et al., 2014; Stumpp et al., 2012, Zhao et al., 2013), but the  
50 choice of lysimeter can affect the portion of soil water (i.e. mobile vs. bound) that is sampled  
51 (Hinkley et al., 2014; Sprenger et al., 2015) and the soil conditions that are sampleable (i.e.  
52 saturation state). Soil water samples collected from both bulk soil samples and lysimeters often  
53 require manual intervention at the time of sampling.

54 Building off of innovations in laser-based spectroscopy for stable isotope geochemistry,  
55 the ecohydrology community developed a variety of in situ soil water sampling methods over the  
56 last 15 years that enable the creation of high throughput, high precision analyses of soil water  
57 isotopes (e.g. Wassenaar et al., 2008; Gupta et al. 2009; Rothfuss et al., 2013; Volkmann and  
58 Weiler, 2014; Gaj et al., 2015; Oerter et al., 2016; Beyer et al., 2020; Kübert et al., 2020). These  
59 methods have provided insights into a range of ecohydrologic questions from evaporation and  
60 water use dynamics in managed soils (e.g. Oerter et al., 2017; Quade et al., 2018) to better  
61 understanding where plants and trees source their water (e.g. Beyer et al., 2020). These  
62 innovations have allowed researchers to ask new questions about ecohydrologic dynamics, but  
63 current methods require field deployments of laser-based instruments. Field deployments are  
64 technically possible and have been conducted successfully (e.g. Gaj et al., 2016; Volkmann et al.,  
65 2016; Oerter et al., 2017; Quade et al., 2019; Künhammer et al., 2021; Seeger and Weiler., 2021;  
66 Gessler et al., 2022), but require uninterrupted AC power, adequate shelter, as well as safe and  
67 stable operating environments for best results. These prerequisites are often unavailable at many  
68 field sites, especially in more remote locations and for longer sampling time frames. Given these  
69 logistical constraints, these studies have mostly been done near the institutions performing those  
70 studies. Spatial constraints limit the questions that researchers can ask about soil hydrology in  
71 remote and traditionally understudied landscapes. For example, in the geoscience community  
72 there is significant interest in improving the research community's understanding of how and  
73 when paleoclimate proxies (e.g. stable isotope records from pedogenic carbonate, branched  
74 glycerol dialkyl glycerol tetraethers, etc.) form in soils, because that informs our ability to  
75 accurately interpret records from the geologic past. However, those projects commonly have  
76 environmental constraints like soil type or local climate characteristics that may not be located  
77 near institutions performing those studies. To be able to study a broader range of questions about  
78 ecohydrology, there is a need for a system that is capable of autonomously collecting soil water  
79 vapor for isotopic analysis in remote settings.

80 In this contribution, we report on the further development and testing of a field  
81 deployable system called the Soil Water Isotope Storage System (SWISS). The SWISS was built  
82 to be paired with ACCURELL PP V8/2HF vapor permeable probes that have been previously  
83 tested for soil water isotope applications (Rothfuss et al., 2013; Oerter et al., 2017). Our system  
84 uses three basic components to store water vapor produced by the vapor permeable probes: glass  
85 flasks, stainless steel tubing and a flask selector valve (Fig. 1, Supplemental Table 1).  
86 Previously, we demonstrated through a series of lab experiments that the glass flasks used in the

87 SWISS units can reliably store water vapor for up to 30 days (Havranek et al., 2020). That proof-  
88 of-concept study demonstrated that the flasks retain original water isotope values, but the  
89 laboratory system was not field deployable and did not have customizable automation. Here, we  
90 present a fully autonomous, field-ready system that has been tested under both laboratory  
91 conditions and field conditions, including development and testing of a solar-powered, battery  
92 backed automation system that enables pre-scheduled water vapor sampling without manual  
93 intervention in remote field locations.

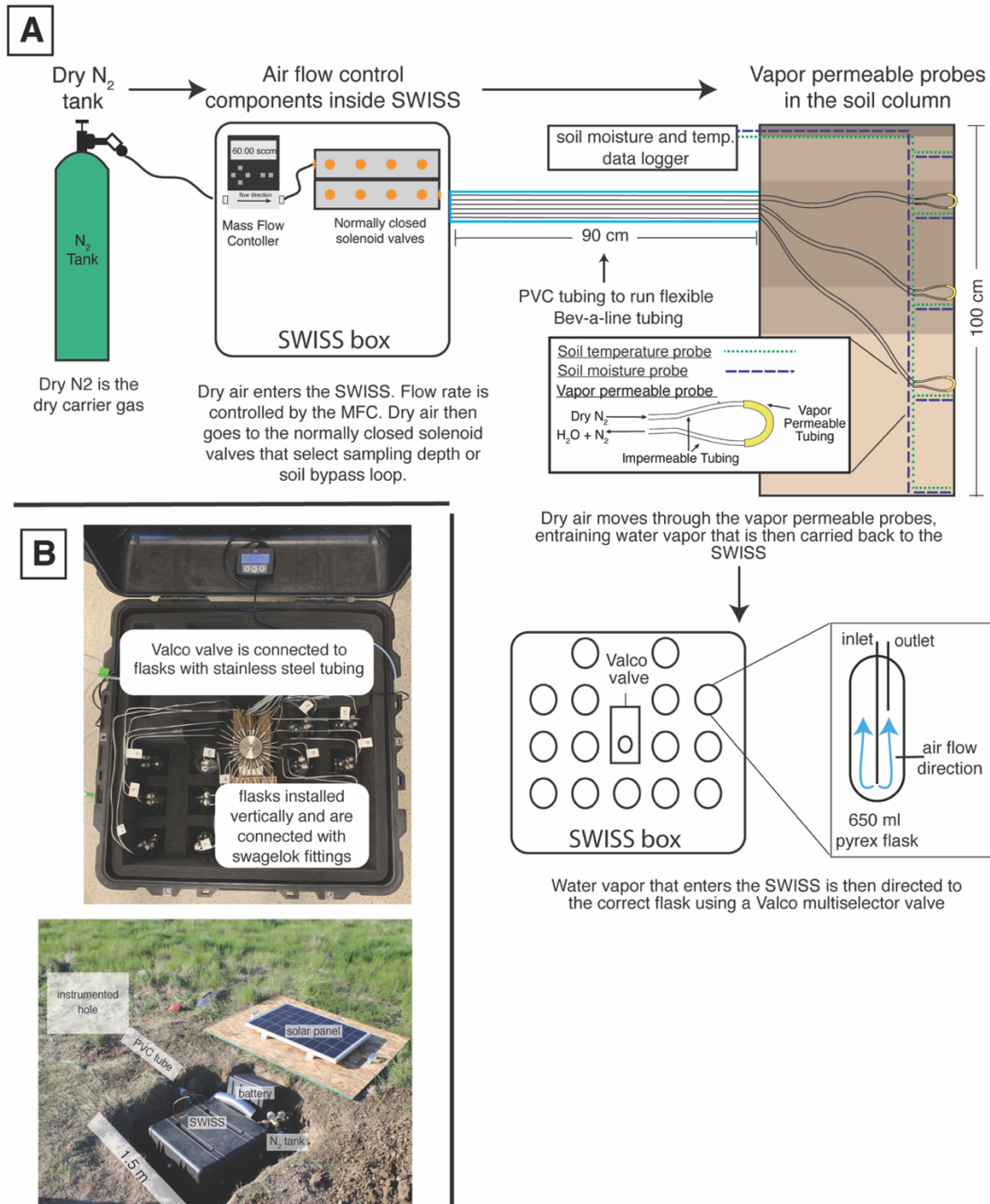
94 To test the accuracy and precision of the SWISS, we completed quality assurance and  
95 quality control (QA/QC) tests. Here, we demonstrate the viability of this system under field-  
96 conditions through two field suitability experiments. In addition, we sampled three different field  
97 sites to show that the automation schema works on a monthly timescale and that the system  
98 preserves soil water vapor isotope signals with sufficient precision to distinguish between three  
99 different field settings and vertical profile differences.

## 100 2 Field Sites

### 101 *2.1 Site Set-Up*

102 At each site we dug two holes; figure 1 shows the field-setup employed at all of our field  
103 sites. One hole was instrumented with soil moisture and temperature data loggers at 25 cm, 50  
104 cm, 75 cm, and 100 cm depths, as well as the water vapor permeable probes at 25 cm, 50 cm and  
105 75 cm depths (Fig 1A). We deployed all probes >9 months before the first samples were  
106 collected to allow the soil to settle and return to natural conditions as much as possible. This  
107 timeframe was longer than other studies (e.g. Kübert et al., 2020) and included infiltration of  
108 spring and early summer precipitation. During probe deployment we took care to retain the  
109 original soil horizon sequence and horizon depths as much as possible. In the second hole, we  
110 stored the SWISS unit, dry nitrogen tank, and associated components to power the SWISS (Fig  
111 1B). The water vapor probes, which connected to the SWISS units with Bev-A-Line  
112 impermeable tubing, were run through a PVC pipe buried at approximately 15 cm depth. We ran  
113 the impermeable tubing underground to limit the effect of diurnal temperature variability on the  
114 impermeable tubing to prevent condensation as water travels from the relatively warm soil to the  
115 SWISS.

116



117  
 118 **Figure 1.** A) The sampling flow path. To sample soil water, dry nitrogen is regulated at a specific rate  
 119 using a mass flow controller, and then directed to one of the three sampling depths, or the soil bypass loop  
 120 using a set of solenoid valves. Both the mass flow controller and solenoid valves are housed inside the  
 121 SWISS. Once directed to the correct sampling depth, dry nitrogen is carried to the vapor permeable  
 122 probes via gas impermeable tubing that is buried approximately 15 cm depth. After passing through the  
 123 vapor permeable probe, the entrained soil water vapor is carried back to the SWISS where it is directed to  
 124 the correct flask using a Valco multiselector valve. B) Photos of a built-out SWISS and the layout of a  
 125 field site. Each of the system components (solar panel, battery,  $N_2$  tank, SWISS, PVC tube) are labeled, in  
 126 addition to the location of the instrumented hole in which all of the probes are buried. The hole which  
 127 houses the SWISS, power, and  $N_2$  tank is approximately 1.5 m wide.

## 128 **2.2 Site descriptions**

129 We deployed the SWISS at three field locations: Oglala National Grassland, Nebraska,  
130 USA; Briggsdale, Colorado, USA; and Seibert, Colorado, USA. The Oglala National Grassland  
131 site (Lat: 42.9600/Long: -103.5979/elev: 1117 m) is located in northwestern Nebraska, USA in a  
132 cold semi-arid climate. The soil at this site is described as an Aridisol with a silt-loam texture. It  
133 is part of the Olney series (Natural Resources Conservation Service, 2022). The Briggsdale site  
134 (Lat: 40.5947/Long: -104.3190/elev: 1480 m) is located in northeastern Colorado, USA in a cold  
135 semi-arid climate. The soil at this site is described as an Alfisol with a loamy sand - sandy loam  
136 texture. It is part of the Olnest series (Natural Resources Conservation Service, 2022). Long term  
137 meteorological data from the Briggsdale site is available from the co-located CoAgMet site  
138 (CoAgMet, Colorado Climate Center). The Seibert site (Lat: 39.1187/Long: -102.9250/Elev:  
139 1479 m) is located in eastern Colorado, USA in a cold semi-arid climate. The soil at this site has  
140 been described as an Alfisol, that has a sand loam texture in the top 50 cm of the profile, and a  
141 silt loam texture between 50 - 100 cm. It is part of the Stoneham series (Natural Resources  
142 Conservation Service, 2022). Long term meteorological data from the site is available from the  
143 co-located CoAgMet site (CoAgMet, Colorado Climate Center).

## 144 **3 Materials**

### 145 **3.1 SWISS Hardware components**

146 In each SWISS there are 15 custom made ~650 ml flasks. These flasks are designed  
147 similarly to those used for other water vapor applications. For example, a similar flask is  
148 currently used in an unmanned aerial vehicle to collect atmospheric water vapor samples for  
149 stable isotope analysis (Rozmiarek et al., 2021). The flasks have one long inlet tube that extends  
150 into the flask almost to the base, and one shorter outlet tube so that vapor exiting the flask is well  
151 mixed and representative of the whole flask (Fig. 1A). The large flask volume is advantageous  
152 because there is a low glass surface area to volume ratio, and therefore we are able to reliably  
153 measure vapor from the flasks on a CRDS instrument without interacting with vapor bound to  
154 the flask walls. The 15 glass flasks are connected to a 16-port, multi-selector Valco valve. We  
155 chose to use a Valco valve because these have previously been shown to sufficiently seal off  
156 sample volumes for subsequent stable isotope analysis (Theis et al., 2004). The valve and flasks  
157 are connected by 1/8 inch stainless steel tubing and stainless steel 1/4 inch to 1/8 inch union  
158 Swagelok fittings; we use PTFE ferrules on the glass flasks with the Swagelok fittings. The first  
159 port of the Valco valve is 1/8 inch stainless steel tubing that serves as a flask bypass loop, which  
160 enables flushing of either dry air or water vapor through the system without interacting with a  
161 flask. All components are contained in a 61 cm x 61 cm x 61 cm Pelican case (Pelican 0370)  
162 with three layers of Pick n' Pluck foam and convoluted foam (Pelican Products Inc., Torrance,  
163 Ca, USA). This case is thermally insulated and provides enough protection to safely transport the  
164 SWISS by vehicle to field sites.

### 166 **3.2 Soil Probes**

167 There are three components for the collection and analysis of soil water vapor: vapor  
168 permeable probes, soil temperature loggers, and soil moisture sensors (Fig 1B, Supplemental  
169 Table 1).

170 Here, we use a vapor permeable membrane (Accurrell PP V8/2HF, 3M, Germany) that  
171 was first tested for soil water isotope applications by Rothfuss et al., (2013). This method works  
172 by flushing dry nitrogen (or dry air) through the vapor permeable membrane, creating a water

173 vapor concentration gradient from inside the probe to the soil, thus inducing water vapor  
174 movement across the membrane. Water vapor is then entrained in the dry nitrogen and flushed to  
175 either a CRDS system or into a storage container. We opted to use this tubing because it has been  
176 shown to deliver reliable data over time (i.e. Rothfuss et al., 2015; Oerter et al., 2019; Kübert et  
177 al., 2020; Seeger and Weiler, 2021; Gessler et al., 2021), and it is easy to use and customize to  
178 individual needs (Beyer et al., 2020; Kübert et al., 2020). We previously observed that variability  
179 in the length of the vapor permeable tubing can lead to systematic offsets in the stable isotope  
180 composition of measured waters that arise from variability of vapor permeable tube surface area  
181 (Havranek et al., 2020). Therefore, we were careful to construct all probes such that the length  
182 of the Accurrell vapor permeable tubing was 10 cm long, and the impermeable Bev-A-Line IV  
183 connected on each side of the vapor permeable tubing was 2 m long. We cut the Bev-A-Line  
184 connections to identical lengths to control for memory effect and to treat all samples identically.  
185 We also constructed the vapor permeable probes to be used in the lab setting for standards in an  
186 identical fashion.

187 Soil temperature loggers (Onset HOBO MX2201), used for applying a temperature  
188 correction to all soil water vapor data and to provide key physical parameters of the soils for  
189 other goals beyond this study, were buried at the same depths as the vapor permeable probes.  
190 Soil moisture sensors (Onset S-SMD-M005) were also buried at the same depths as the vapor  
191 permeable probes.

192

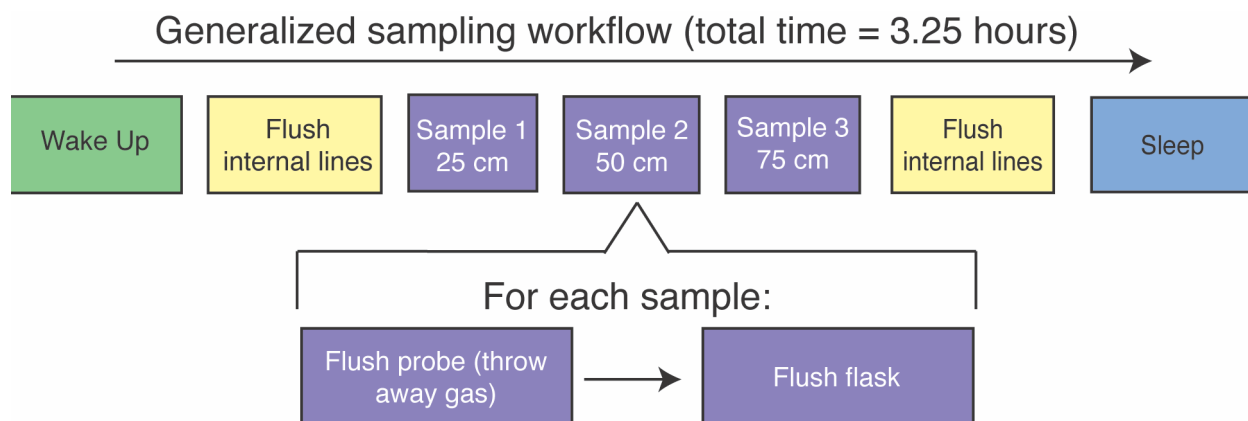
### 193 **3. 3 Automation components, code style, and remote setting power**

194 The philosophy behind the automation of the SWISS was to make it as easy to reproduce  
195 as possible, and as flexible as possible to meet different users' sampling needs. We therefore use  
196 widely available hardware components and electronics parts; for each product there are  
197 numerous alternatives which should be equally viable and could be swapped to better meet each  
198 user's needs. In an effort to make our system as accessible and customizable as possible for the  
199 scientific community, all automation code is completely open source and will continue to be  
200 refined for future applications and hardware improvements. We note that all code is provided as-  
201 is and should be tested carefully for use in other experiments.

202 The overall sampling scheme used in this paper is described in figure 2 and table 1. Our  
203 experimental goal was to create a time series of soil water vapor data from three discrete  
204 sampling depths (25 cm, 50 cm, 75 cm). Prior to sampling any soil water vapor, we bypassed the  
205 soil probes and flushed the lines within the SWISS. Then, at the start of sampling for each depth,  
206 we also flushed the water vapor probe to remove condensation or 'old' water vapor. The gas  
207 from both of those steps was expelled via the flask bypass loop. Each soil depth was then  
208 sampled for 45 minutes by flushing through the next flask designated in the sequence.

209 Supplemental figure 1 shows the components of the automation system. To automate and  
210 program the sampling scheme, we used: (1) a microcontroller to run the automation script; (2) a  
211 coin-cell battery powered real time clock so that the microcontroller was always capable of  
212 keeping track of time through power losses, and therefore maintain the sampling schedule; (3) an  
213 RS-232 to TTL converter for serial communication with the Valco valve; (4) solenoid valves that  
214 were used to control which depth was being sampled and the associated direct current (VDC)  
215 power relay; (5) a mass flow controller used to control the rate at which dry nitrogen (1 ppm  
216 H<sub>2</sub>O) is flushed through the probes; and (6) a power relay used to power the Valco valve and  
217 mass flow controller. All parts are described in detail in Supplemental Table 2.

218



219  
220 **Figure 2.** Flow chart of the instrument schedule used for sampling during all field experiments.  
221

222 **Table 1.** Description of soil water sampling steps

Code Step	Wake-up	Flush internal lines	Flush depth 1	Sample depth 1	Flush depth 2	Sample depth 2	Flush depth 3	Sample depth 3	Flush internal lines	sleep
time (minutes)	1	15	10	45	10	45	10	45	15	1
Valco valve position	flask bypass	flask bypass	flask bypass	2, 5, 8, 11, or 14	flask bypass	3, 6, 9, 12, or 15	flask bypass	4, 7, 10, 13, or 16	flask bypass	flask bypass
solenoid valve position	none	soil bypass	25 cm	25 cm	50 cm	50 cm	75 cm	75 cm	soil bypass	none

223  
224 In a remote setting, the SWISS units are powered using the combination of a 12 volt  
225 deep-cycle battery with a 12VDC, 100 watt solar panel that is used to charge the battery. The  
226 solar panel is mounted to a piece of plywood that covers the hole where the SWISS is deployed  
227 (note, the hole is uncovered in Fig. 1B for illustrative purposes). We opted for this setup because  
228 the underground storage of all parts of the system creates a discreet field site that attracts  
229 minimal attention from other land users, and helps reduce exposure to temperature and  
230 precipitation extremes. In the field, we used a 12VDC-120VAC power inverter to provide simple  
231 plug and play power for the Valco valve and mass flow controller. This simple combination was  
232 suitable for summertime in the Western U.S. where there are many hours of direct sunlight, and  
233 the solar panel was able to easily charge the 12V battery. This setup may need to be adjusted  
234 based on location and desired sampling time. Like the automation system, there are many  
235 commercial options available for products, and they can be easily adjusted for users' needs;  
236 example parts are described in detail in Supplemental Table 2. We also note that in areas where it  
237 is possible to plug into a power grid, the deep cycle battery, solar panel and power inverter can  
238 be removed.

239 **4. Methods**

240 We completed all water vapor isotope analyses in the Stable Isotope Lab at the Institute  
241 of Arctic and Alpine Research (INSTAAR SIL) at the University of Colorado Boulder between  
242 October 2020 and August 2022. We used a Picarro L-2130i water isotope analyzer (Picarro, Inc.  
243 Santa Clara, CA) to measure both water concentration and the oxygen and hydrogen isotope  
244 ratios of the water vapor.

245  
246 **4.1 QA/QC: Testing the SWISS under lab conditions**

247 Our highest order concern for the SWISS is that it remains leak-free, because leaks would  
248 introduce the potential for fractionation or mixing of atmosphere that would alter the stable  
249 isotope ratio of the water vapor in the flask. To mitigate leaks, we developed a three-part quality  
250 assurance and quality control (QA/QC) procedure that must be completed for each new SWISS  
251 prior to the first deployment. The first step detects any large, fast leaks using helium detection  
252 methods; the second step detects medium scale leaks using dry air; and the third step detects  
253 slow, small scale leaks using water vapor tests. Full procedural descriptions are available in the  
254 supplemental material and the data processing code is available via GitHub.

255  
256 **4.1.1 Step 1: Use helium to detect large, fast leaks**

257 After initial assembly of the SWISS units, we looked for large leaks from the cracking of  
258 inlet or outlet tubes on the glass flasks that occasionally occurred while tightening the Swagelok  
259 fittings. To do this, we filled the flasks with helium and used a helium leak detector (Leak  
260 Detector, Catalog #22655, Restek, Bellefonte, PA, USA). Another easy alternative to a helium  
261 leak test is to complete a very short dry air test (methods described below) where the hold-time is  
262 on the order of 12-24 hours.

263  
264 **4.1.2 Step 2: Use dry air to detect medium scale leaks**

265 The goal of this test was to catch any second order, medium-scale leaks associated with  
266 either Valco valve fittings or Swagelok fittings that were under tightened.

267  
268 *Step 2A: Fill flasks with dry air*

269 To start every experiment, we filled flasks with air that is filtered through Drierite (which  
270 has a water vapor mole fraction of less than 500 ppm), at 2 L/min for 5 minutes. With a flask  
271 volume of 650 ml, this means the volume of the flask is turned over 15 times.

272  
273 *Step 2B: Hold period*

274 Flasks were then sealed and left to sit for seven days. This time period can be adjusted by  
275 other users to fit their climate or needs.

276  
277 *Step 2C: Measure water vapor mole fraction using dead-end pull sample introduction*

278 At the end of the seven-day period, we measured each flask using a dead-end pull sample  
279 introduction method. For this sample introduction method, the inlet to the Valco valve was  
280 sealed with a 1/4 inch Swagelok cap and there was no introduction of a carrier gas. As a result,  
281 air was removed from the flask based on the flow rate of the Picarro analyzer (typically 27 - 31  
282 ml/min). Flasks were measured for five minutes, which resulted in ~150 ml of air being removed  
283 from the flasks. All components within the SWISS are capable of being fully evacuated. Water  
284 vapor mole fractions determined by Picarrros are not standardized, so it is impossible to know for



285 sure the exact magnitude of water vapor mole fraction change between the input analysis and the  
286 final value at the end of the dry air test. However, these instruments are remarkably stable over  
287 weeks, and so the relative changes observed (e.g. increase or decrease of mole fraction relative to  
288 the initial amount) are likely reliable, particularly for the larger magnitude changes.

289 If a flask had a water vapor mole fraction of less than 500 ppm, it “passed” step 2 of  
290 QA/QC. If a flask had a water vapor mole fraction greater than 500 ppm, it “failed” step 2 of  
291 QA/QC, and we tightened both the Swagelok connections on the flasks as well as the fittings  
292 between the stainless steel tubing and the Valco valve. We repeated dry air tests on any given  
293 SWISS unit until the majority (typically at least 13/15) of the flasks had passed step 2 of QA/QC.  
294

#### 295 **4.1.3 Step 3: Water vapor tests detect small scale leaks**

296 The purpose of this experiment was to mimic storage of water vapor at concentrations  
297 similar to what we might expect in a soil, and for durations similar to those of our field  
298 experiments. These experiments were meant to test whether flasks filled early in the sampling  
299 sequence during field deployments leak by the time samples are returned to the lab for  
300 measurement. For this experiment, we filled flasks with water vapor of known isotopic  
301 composition and water vapor mole fraction, sealed the flasks for 14 days, and then measured the  
302 water vapor mole fraction and isotope values of each flask. We performed 11 water vapor tests  
303 that were done across three analytical sessions using six different SWISS units. Across these  
304 three sessions, we measured 164 flasks both at the start of the 14-day experiment, and at the end.  
305

##### 306 *Step 3A: Flush flasks with dry air*

307 Prior to putting any water vapor into the flasks (either in the field or in the lab), we  
308 completed a dry air fill (as described in QA/QC step 2A) that served to purge the flasks of any  
309 prior water vapor that might exchange with the new sample.  
310

##### 311 *Step 3B: Fill flasks with water vapor and measure input isotope values*

312 To supply water vapor to the flasks, we used the vapor permeable probes that were  
313 constructed identically to those deployed in the field. We immersed the probes up to the  
314 connection between the vapor permeable and impermeable tubing in water, taking care to not  
315 submerge the connection point and inadvertently allow liquid water to enter the inside of the  
316 vapor permeable tubing. We flushed the flasks at a rate of 150 ml/min for 30 minutes, and  
317 measured the  $\delta^{18}\text{O}$  and  $\delta^2\text{H}$  values and mole fraction of water vapor as each flask was filled. To  
318 fill 15 flasks sequentially, the probes were submerged in water for approximately 7.5 hours.

319 Across three different sessions, we used three different waters that are tertiary standards  
320 in the INSTAAR SIL to complete these experiments: a light water made from melting and  
321 filtering Rocky Mountain snow ( $\sim -25.5\text{‰}$  and  $-187.5\text{‰}$  VSMOW, for  $\delta^{18}\text{O}$  and  $\delta^2\text{H}$ ,  
322 respectively), an intermediate water that is deionized (DI) water from the University of Colorado  
323 Boulder Campus ( $\sim -16.2\text{‰}$  and  $-120.7\text{‰}$  VSMOW for  $\delta^{18}\text{O}$  and  $\delta^2\text{H}$ , respectively) and a heavy  
324 water that is filtered water sourced from Florida, USA ( $\sim -0.8\text{‰}$  and  $-2.8\text{‰}$  VSMOW for  $\delta^{18}\text{O}$   
325 and  $\delta^2\text{H}$ , respectively). All tertiary lab standards are characterized relative to international  
326 primary standards obtained from the International Atomic Energy Agency and are reported  
327 relative to the V-SMOW/SLAP standard isotope scale. To calculate the input value, we averaged  
328  $\delta^{18}\text{O}$  and  $\delta^2\text{H}$  values over the last three minutes of the filling period. We then stored the water  
329 vapor in the flasks for 14 days. At the end of the 14-day storage period, we measured each flask  
330 to evaluate if the  $\delta^{18}\text{O}$  and  $\delta^2\text{H}$  values had significantly changed over the storage period.

331

332 *Step 3C: Measure the water vapor isotope values*

333 To mitigate memory effects between flasks, we ran dry air via the flask bypass loop (port  
334 one of every SWISS unit) for five minutes between each flask measurement. To verify that the  
335 impermeable tubing between the SWISS and the Picarro was sufficiently dried, we waited until  
336 the water vapor mixing ratio being measured by the Picarro was below 500 ppm for >30 seconds.

337 During this five-minute window, we used a heat gun to manually warm each flask. We  
338 believe heating the flasks creates a more stable measurement by limiting water vapor bound to  
339 the glass walls of the flask and by helping to homogenize the water vapor within the flask. While  
340 we did not strictly control or regulate the temperature of the flasks, they were all warm to the  
341 touch.

342 Once we warmed the flask and dried the impermeable tubing, water vapor was introduced  
343 to the CRDS using one of two methods: 1) the dead-end pull sample introduction method  
344 described above, or 2) a *dry air carrier gas sample introduction* method. During the dry air  
345 carrier gas sample introduction method, dry air is continuously flowing through the flask at a rate  
346 of 27-31 ml/min for the entire 12-minute measurement period. To reach a water vapor mole  
347 fraction of approximately 25,000 ppm (the optimal humidity range for the Picarro L2130-*i*), we  
348 diluted the water vapor with dry air at a rate of 10 ml/min. Without dilution, the concentration  
349 out of the flasks is as high as 35,000 - 40,000 ppm, which leads to linearity effects on a Picarro  
350 L2130-*i* that can be challenging to correct for. The dead-end pull method is preferable when the  
351 water vapor mole fraction inside the flask is low (<17,000 ppm), because there is no additional  
352 introduction of dry air. The introduction of dry air decreases the water vapor mole fraction  
353 throughout the measurement, and in fairly dry flasks, using the dry air carrier gas method can  
354 lower the water vapor mole fraction to below 10,000 ppm. Below 10,000 ppm, there are large  
355 linearity isotope effects associated with the measurement on a Picarro L2130-*i*, and the isotope  
356 values are challenging to correct into a known reference frame, just as with high water vapor  
357 mole fractions. The major downside of the dead-end pull method is that condensation is more  
358 likely to form in the stainless steel tubing that connects the flasks to the Valco valve, as well as  
359 the Valco valve itself, compared to the dry air carrier gas method. The dry air carrier gas method  
360 prevents condensation from forming in the Valco valve and tubing, and prevents fractionation  
361 that may occur because of changing pressure within the flask. It is possible that during a dead-  
362 end pull on the flask, heavier isotopes may remain attached to the walls of the flask, coming off  
363 later as the pressure drops. For these reasons, the dry air carrier gas sample introduction method  
364 is our preferred method for sample introduction in most cases.

365 For each flask, we looked at the stability of the isotope values as well as either a stable  
366 water vapor mole fraction if the dead end pull method was being used or a steady, linear decrease  
367 in water vapor mole fraction if the dry air carrier gas method was being used. For approximately  
368 90% of the flasks we found that after excluding the first three minutes of measurement of each  
369 flask, the subsequent three minutes were the most stable. For the remaining ~10% of the flasks,  
370 using a time window that started either ~30 seconds earlier or ~30 seconds later to create an  
371 average isotope value offered a more stable isotope signal with smaller instrumental  
372 uncertainties. Any flask that required specialized treatment during the data reduction process was  
373 flagged during measurement.

374

375 *Step 3D: Data correction*

376 During these experiments, we monitored instrument performance (e.g. drift) in two ways.  
377 First, to run standards identically to how samples were collected, we introduced tertiary  
378 standards, described above, using vapor probes. The water vapor produced by the vapor  
379 permeable probes was flushed through the SWISS unit via the flask bypass loop and diluted with  
380 a 10 ml/min dry air flow to reach a water vapor mole fraction of approximately 25,000 ppm  
381 before entering the Picarro. Second, we introduced a suite of four secondary standards that have  
382 been calibrated against primary standards, and reported against VSMOW/SLAP via a flash  
383 evaporator system described in detail by Rozmiarek and others (2021). This flash evaporator  
384 system can be used to adjust the water vapor mole fraction to create linearity corrections at high  
385 and low water vapor mole fractions. After correcting data into a common reference frame, we  
386 calculated the difference between the input isotope values and the ending isotope values.

387 The results of these tests were used to carefully document flasks that do not perform well,  
388 and any idiosyncrasies of SWISS units. That way, during field deployment suspicious those  
389 flasks could be easily identified and investigated.

390

## 391 **4.2 Field suitability experiments:**

### 392 ***4.2.1 Field suitability experiment #1: Long term field dry air test***

393 As a complement to the QA/QC we did under lab conditions, we also completed long  
394 term dry air tests at our field sites. We had three goals associated with these experiments. The  
395 first was to test whether, even under field conditions, where daily temperature and relative  
396 humidity fluctuations are different than in a lab setting, the flasks were still resistant to  
397 atmospheric intrusion. Second, we used these tests to evaluate whether the flasks that were  
398 flushed with soil water vapor near the end of a sampling sequence took on atmosphere prior to  
399 sampling. Lastly, we chose these time intervals because they bracket the typical length of a  
400 deployment, which helped us determine how quickly flasks should be measured after bringing a  
401 SWISS back to the lab.

402 Like all field deployments, we started with a dry air fill, and then one SWISS unit was  
403 deployed to each of our three field sites. No soil water was collected during these deployments.  
404 The duration between filling the flasks with dry air to measuring the flasks was between 34 - 52  
405 days. The 34 and 52 day tests were done during June 2022 and August 2021, respectively, and  
406 therefore tests the SWISS under warm summertime conditions. The 43 day test was done in  
407 October 2021, which included nights where air temperatures fell below 0°C. The only barrier  
408 between air and the SWISS in its deployment hole was a plywood board, and so this deployment  
409 tested the suitability of the SWISS to maintain integrity under freezing conditions.

410

### 411 ***4.2.2. Field suitability experiment #2: Mock field tests***

412 To test whether the automation code and sampling scheme we developed worked as  
413 expected on short, observable timescales, we set up an experiment to simulate field deployment  
414 of one SWISS unit (Meringue) near the University of Colorado Boulder. This test applied the  
415 automation components and remote power setup described in the materials section. During this  
416 field-simulation experiment, our goal was to collect three discrete samples each sampling period,  
417 to simulate the collection of water vapor from three soil depths. An important goal of this test  
418 was to test whether the sampling scheme introduced any memory effects between samples. We  
419 followed the sampling protocol described in figure 2 and table 1.

420 The day before the experiment began, all flasks were flushed with dry air as described in  
421 section 4.1.2. Over the course of 25 hours, all 15 flasks were filled with three different vapors

422 according to a set schedule as would be done in the field. Two of the vapors were created by  
423 immersing the water vapor permeable probes in the  
424 light water and intermediate water as described in section 4.1.3. The third was water vapor from  
425 the ambient atmosphere. All three vapors were sampled using vapor permeable probes  
426 constructed identically to those deployed in the field. For this experiment, we filled three flasks  
427 per cycle with each one of the waters (e.g. Flask 2 = light, Flask 3 = intermediate, Flask 4 =  
428 atmosphere). The choice to sample atmosphere alongside two waters reflects our second goal of  
429 this test, which was to demonstrate that sampled water vapor isotope values do not drift towards  
430 atmospheric values (Magh et al., 2022).

431 Following the sampling schedule, we stored the SWISS unit in a simulated field setting  
432 for seven days. At the end of the seven days, we measured the flasks. For flasks that had a high  
433 water vapor mole fraction (i.e. light and intermediate water vapor samples) we used the dry air  
434 carrier gas sample introduction method. For flasks that had a low water vapor mole fraction (i.e.  
435 atmosphere, ~15,000 ppm) we used the dead end pull sample introduction method.

436 To create average values for each flask, we followed the same averaging protocol  
437 described in section 4.1.3. We used equations 2A and 2B from Rothfuss et al., (2013) to convert  
438 from water vapor to liquid values. Then, using secondary and tertiary standards, data were  
439 corrected into the VSMOW isotope scale. Finally, the SWISS unit offset correction (detailed  
440 below in section 6.1.2) was applied.

441

#### 442 ***4.3 Example Field Deployment: One month period***

443 We deployed one SWISS unit each to the three field sites described in summer 2022.  
444 Before deployment, all SWISS units were flushed with dry air following the protocol outlined in  
445 section 4.1.2. Flasks were flushed with dry air one to three days prior to field deployment. At  
446 each site, we sampled at three depths (25 cm, 50 cm, and 75cm) on each sampling day, following  
447 the protocol described in figure 2 and table 1. We sampled soil water from all three depths every  
448 five days (protocol length = 25 days total). At Oglala National Grassland, samples were taken  
449 every five days from 2022-06-25 to 2022-07-14. At the Briggsdale, CO site samples were taken  
450 every five days between 2022-07-17 and 2022-08-06. At the Seibert, CO site, samples were  
451 collected every five days between 2022-06-19 and 2022-07-04. At the end of a 28-day period,  
452 the SWISS units were returned to the lab, and measured. SWISS units were measured within five  
453 days of returning from the field. The maximum number of days a flask held sample water vapor  
454 during these deployments was 32 days. The measurement protocol and data averaging protocol  
455 follows the procedures described in section 4.1.3. The data correction scheme follows as in the  
456 section 4.2.2.

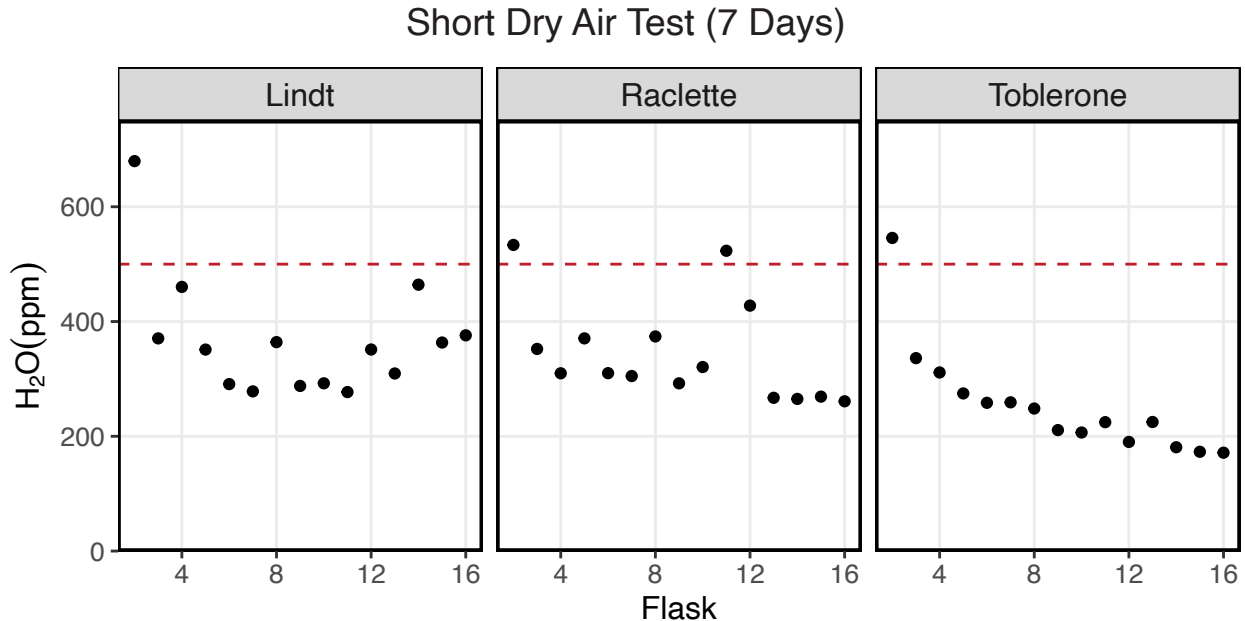
## 457 **5 Results**

### 458 **5.1 QA/QC Results**

#### 459 ***5.1.1 Dry air test***

460 Figure 3 shows the results of a seven-day dry air test for three SWISS units (marked by  
461 the unit name) (SI Table 3). For all three SWISS units, at least 13/15 of the flasks maintained a  
462 water vapor mole fraction value of less than 500 ppm over the seven-day period. In two of the  
463 three SWISS units (Lindt and Raclette), the water vapor mole fraction for flasks was randomly  
464 distributed around approximately 350 ppm. In Toblerone there was a systematic decrease in  
465 water vapor mole fraction from flask two through flask 16, matching the order in which the

466 flasks were filled with dry air initially. In all three SWISS units, flask two had the highest water  
 467 vapor mole fraction of all the flasks. Supplemental figure 2 shows the results of successive dry  
 468 air tests on the SWISS unit Toblerone where Swagelok fittings were tightened between tests.  
 469 There was a significant decrease in measured water vapor mole fraction for many flasks, but  
 470 particularly for flasks 10 and 11 as a result of tightening the fittings.



471  
 472 **Figure 3. Results of a dry air test from three different SWISS units named: Lindt, Raclette and Toblerone. The majority**  
 473 **of the flasks maintain a water vapor mixing ratio of less than 500 ppm.**  
 474

475 **5.1.2. Water vapor test**

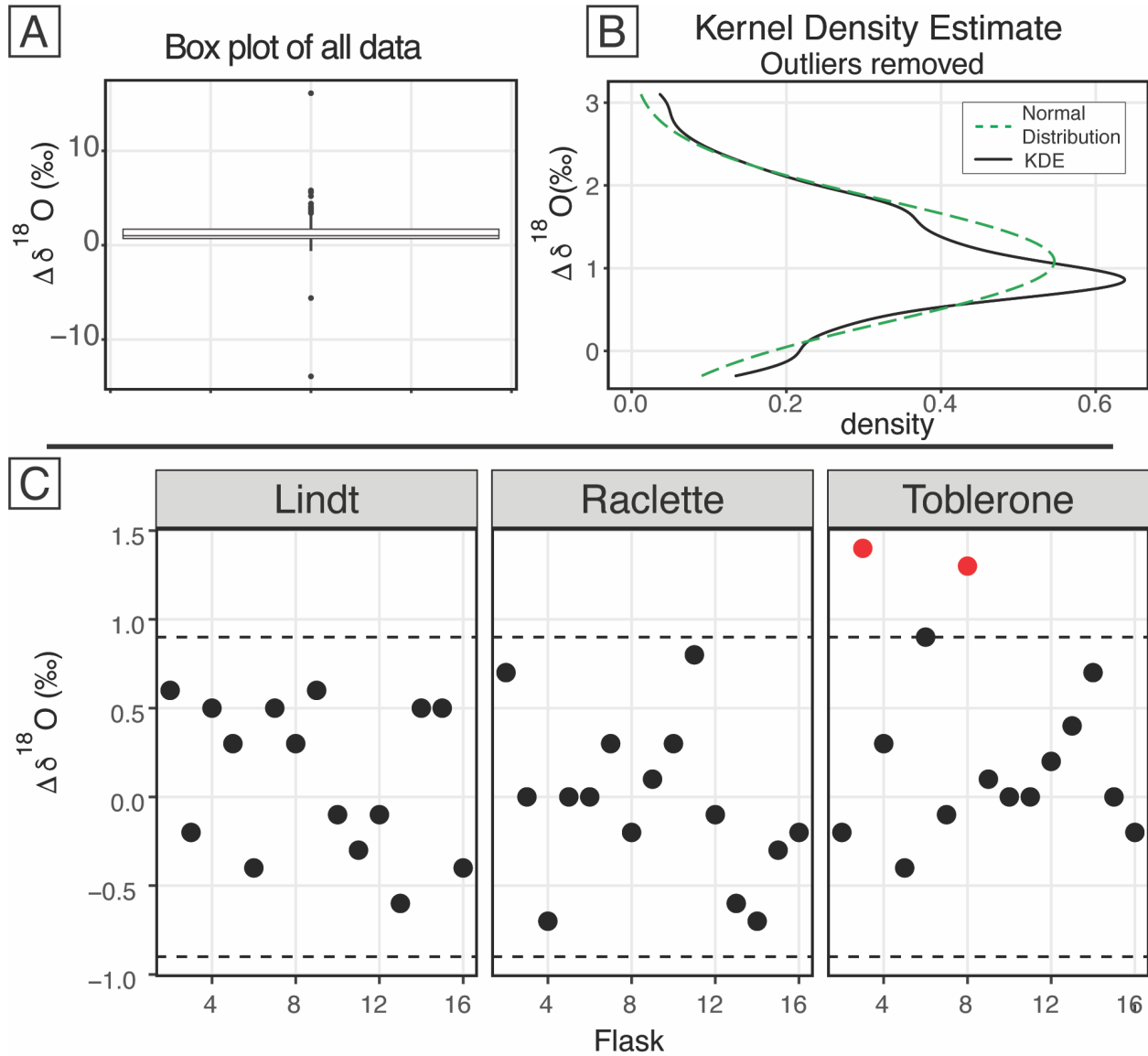
476 Figure 4 shows the  $\delta^{18}\text{O}$  results of 11 water vapor tests performed using six different  
 477 SWISS units. Ideally, we expect a normal distribution centered about 0 within the uncertainty  
 478 limits of the water vapor probes (Oerter et al., 2016). For  $\delta^{18}\text{O}$ , the mean difference between the  
 479 start and end values for the flasks is 1.1‰ with a standard deviation of 0.72‰ (outliers  
 480 removed). There is a consistent positive offset, with a few clear outliers (Fig. 4A). We do not  
 481 observe a consistent difference between water vapor sample introduction methods (Supplemental  
 482 Fig. 3). After removing outliers ( $< Q1 - 1.5 \cdot IQR$  or  $> Q3 + 1.5 \cdot IQR$ ,  $n = 15$ ) from the dataset,  
 483 we compared the kernel density estimate shape to a normal distribution calculated from the mean  
 484 and standard deviation of the dataset to assess dataset normality (Fig. 4B). A normal distribution  
 485 slightly overestimates the center of the data, but captures the overall shape fairly well. Therefore,  
 486 we used the median offset (1.0‰) to correct our water vapor isotope values, and used the  
 487 interquartile range of the dataset (outliers removed) to estimate uncertainty of the SWISS as  $\pm$   
 488 0.9‰. In figure 5C, for simplicity, we just present the results from 45 flasks (three SWISS  
 489 units), with the 1.0‰ offset correction applied. After correction, data are randomly distributed  
 490 about 0, and are within the uncertainty range of  $\pm 0.9\%$  (Supp. Table 4).

491 Figure 5 shows the  $\delta^2\text{H}$  results of 11 water vapor tests. For  $\delta^2\text{H}$ , the mean difference  
 492 between the start and end values is 2.63‰ with a standard deviation of 2.85‰ (outliers  
 493 removed). Similar to  $\delta^{18}\text{O}$ , we expected a normal distribution of differences centered around 0.  
 494 As with  $\delta^{18}\text{O}$ , there was a consistent positive offset with some outliers (i.e.,  $< Q1 - 1.5 \cdot IQR$  or  $>$   
 495  $Q3 + 1.5 \cdot IQR$ ) (Fig. 5A). After removing outliers ( $n = 26$ ) from the dataset, we compared the

496 kernel density estimate to a normal distribution calculated from the mean and standard deviation  
497 of the dataset to assess dataset normality (Fig. 5B). As with  $\delta^{18}\text{O}$ , the center of the dataset is  
498 overestimated by the mean, but the overall peak shape is roughly captured. We therefore use the  
499 median value of 2.3‰ as an offset correction and estimate uncertainty at  $\pm 3.7\%$  for  $\delta^2\text{H}$  from the  
500 interquartile range. In figure 5C, we present the results from 45 flasks (three SWISS units), with  
501 the 2.3‰ offset correction applied. Data are randomly distributed about 0 and are within the  
502 uncertainty range of  $\pm 3.7\%$  (Supplemental Table 4).

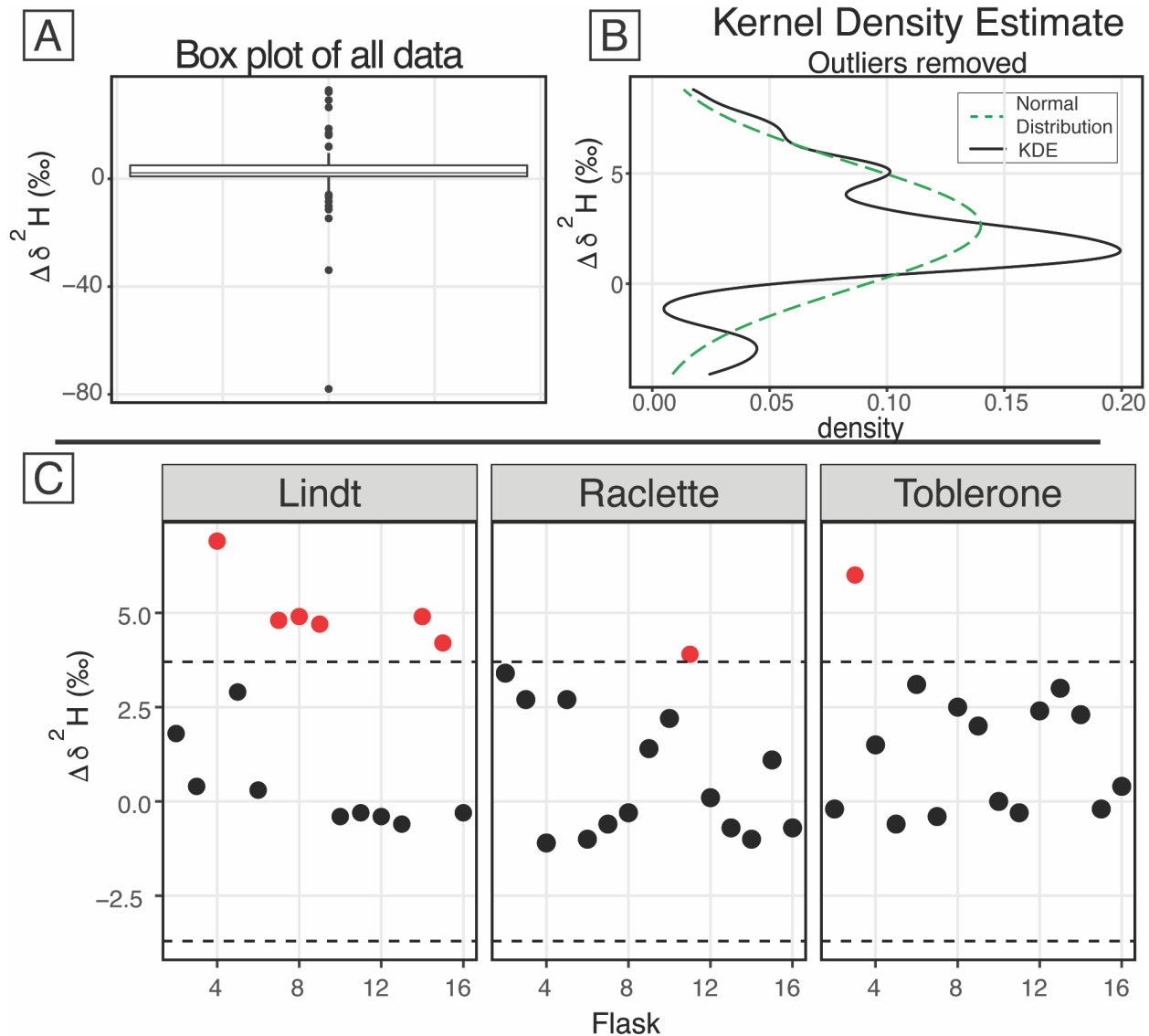
503         When we compared the results in figures 4C and 5C, we found that flasks that performed  
504 adequately for  $\delta^{18}\text{O}$  did not always perform adequately for  $\delta^2\text{H}$ . The results from the SWISS unit  
505 Lindt display this behavior particularly well. Less commonly, some flasks that were within  
506 uncertainty of the system for  $\delta^2\text{H}$  were not within uncertainty of the system for  $\delta^{18}\text{O}$ , like flask 8  
507 in the SWISS unit Toblerone (Figs. 4C, 5C). In a dual isotope plot, there is a strong positive  
508 correlation between  $\delta^2\text{H}$  and  $\delta^{18}\text{O}$  with a slope of 3.14 and an  $R^2$  value of 0.62 (Supplemental  
509 Fig. 4).

510



512  
513  
514  
515  
516  
517  
518  
519  
520  
521  
522  
523  
524

**Figure 4.**  $\delta^{18}\text{O}$  results of the water vapor tests. A) Boxplot of the difference between the starting  $\delta^{18}\text{O}$  value and the final  $\delta^{18}\text{O}$  value of all 164 flasks. B) After removing the outliers from the dataset, the kernel density estimate (black line) and the normal distribution calculated from the dataset (dashed green) are shown. C) After applying the offset correction of 1.0‰, the difference between the starting  $\delta^{18}\text{O}$  value and the final  $\delta^{18}\text{O}$  value for three boxes from the August 2022 session are shown. An uncertainty of  $\pm 0.9\text{‰}$  is marked with a dashed line, and data points that fall outside that uncertainty are colored red.



525  
 526  
 527 **Figure 5.**  $\delta^2\text{H}$  results of the water vapor tests A) Boxplot of the difference between the starting  $\delta^2\text{H}$  value and the final  $\delta^2\text{H}$  value  
 528 of all 164 flasks. B) After removing the outliers from the dataset, the kernel density estimate (black line) and the normal  
 529 distribution calculated from the dataset (dashed green) are shown. C) The difference between the starting  $\delta^2\text{H}$  value and the final  
 530  $\delta^2\text{H}$  value for three boxes from the August 2022 session are shown after applying the offset correction of 2.3‰. An uncertainty of  
 531  $\pm 3.7\%$  is marked with a dashed line, and data points that fall outside that uncertainty are colored red.  
 532



533 **5.2 Field suitability test results**

534 **5.2.1 Dry air test**

535 Figure 6A shows the result of placing three different SWISS units that were flushed with  
536 dry air out into the field for 34 - 52 days (SI Table 3). This timescale (4-6 weeks) is similar to  
537 most field deployments. At the timescale of 34 - 43 days, 13 of the 15 flasks typically maintained  
538 a water vapor mole fraction of less than 1000 ppm. Over the 52 days, seven flasks maintained a  
539 water vapor mole fraction less than 1000 ppm and the remaining 8 had a water vapor mole  
540 fraction between 1000 - 2500 ppm.

541

542 **5.2.2 Automation test**

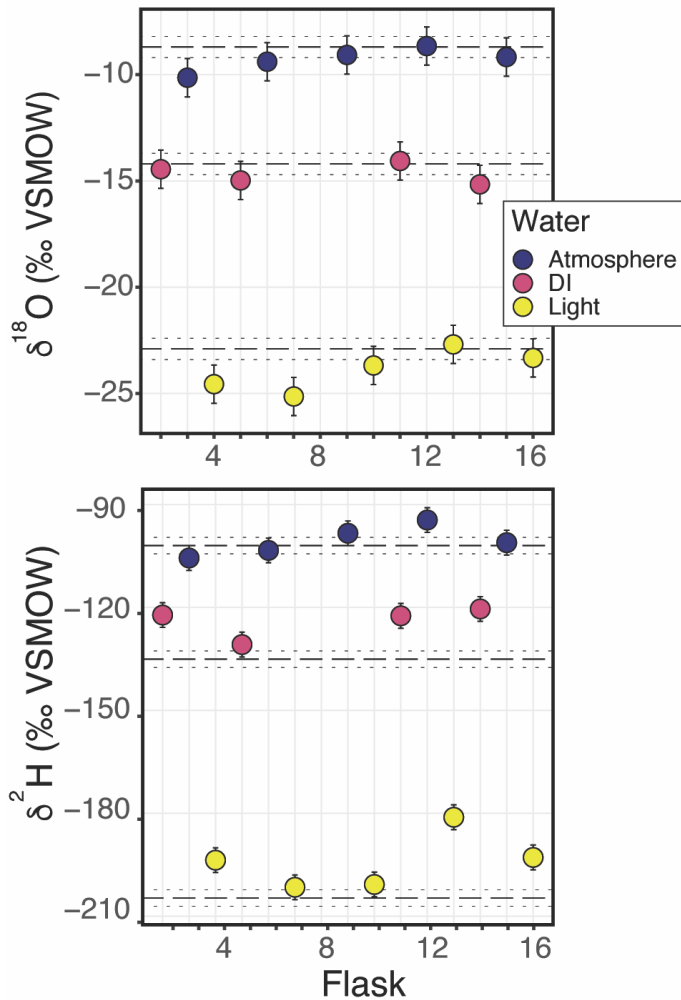
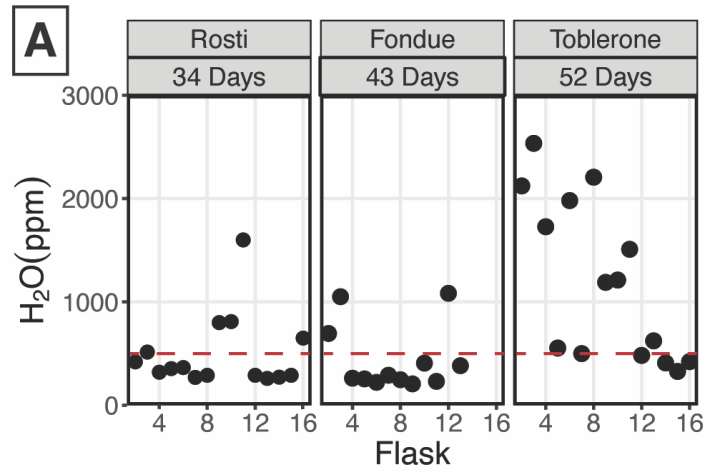
543 Figure 6B shows the results of using the automation code to collect and store water vapor  
544 of known composition for seven days (Table 2). In both plots, the known values of the water are  
545 shown as a long-dash line. Uncertainty on those measurements is estimated at  $\pm 0.5\text{‰}$  and  $\pm 2.4\text{‰}$   
546 for  $\delta^{18}\text{O}$  and  $\delta^2\text{H}$ , respectively (Oerter et al., 2016), shown as the dotted lines. We estimated the  
547 isotope value of the atmosphere at the time of sampling with water vapor mole fraction,  $\delta^{18}\text{O}$ ,  
548 and  $\delta^2\text{H}$  data from the CRDS in the lab. The isotope value, that was corrected as described in  
549 section 4.2.2, of each flask is shown, with uncertainty associated with the SWISS units estimated  
550 at  $\pm 0.9\text{‰}$  and  $\pm 3.7\text{‰}$  for  $\delta^{18}\text{O}$  and  $\delta^2\text{H}$ , respectively.

551 Seven of the nine flasks filled with flash-evaporated water vapor overlap within  
552 uncertainty of the known  $\delta^{18}\text{O}$  value for those standards (top plot, Fig. 6B), and four of the five  
553 flasks filled with atmospheric vapor overlap within uncertainty of our estimated  $\delta^{18}\text{O}$  value.  
554 Flasks that fall outside of the bounds of uncertainty have lower  $\delta^{18}\text{O}$  values than the expected  
555 value. For  $\delta^2\text{H}$ , (bottom plot, Fig. 6B) only three of the nine flasks filled with flash-evaporated  
556 water vapor overlap within uncertainty of the known value of those standards, while four of the  
557 five flasks filled with atmospheric vapor overlap within uncertainty of the estimated  $\delta^2\text{H}$  value.  
558 Flasks that fall outside of the bounds of uncertainty have higher  $\delta^2\text{H}$  values than the expected  
559 value.  
560

561 **Table 2.** Results of the Automation test

<b>SWISS</b>	<b>Flask</b>	<b>water</b>	<b>δ<sup>18</sup>O (‰)</b>	<b>δ<sup>2</sup>H (‰)</b>
Meringue	2	DI	-14.4	-122.2
Meringue	3	Atmosphere	-10.1	-105.6
Meringue	4	Light	-24.6	-193.7
Meringue	5	DI	-15.0	-130.8
Meringue	6	Atmosphere	-9.4	-103.4
Meringue	7	Light	-25.1	-201.5
Meringue	8	DI	-17.3	-140.5
Meringue	9	Atmosphere	-9.1	-98.4
Meringue	10	Light	-23.7	-200.7
Meringue	11	DI	-14.1	-122.5
Meringue	12	Atmosphere	-8.7	-94.5
Meringue	13	Light	-22.7	-181.2
Meringue	14	DI	-15.2	-120.5
Meringue	15	Atmosphere	-9.2	-101.1
Meringue	16	Light	-23.3	-192.9

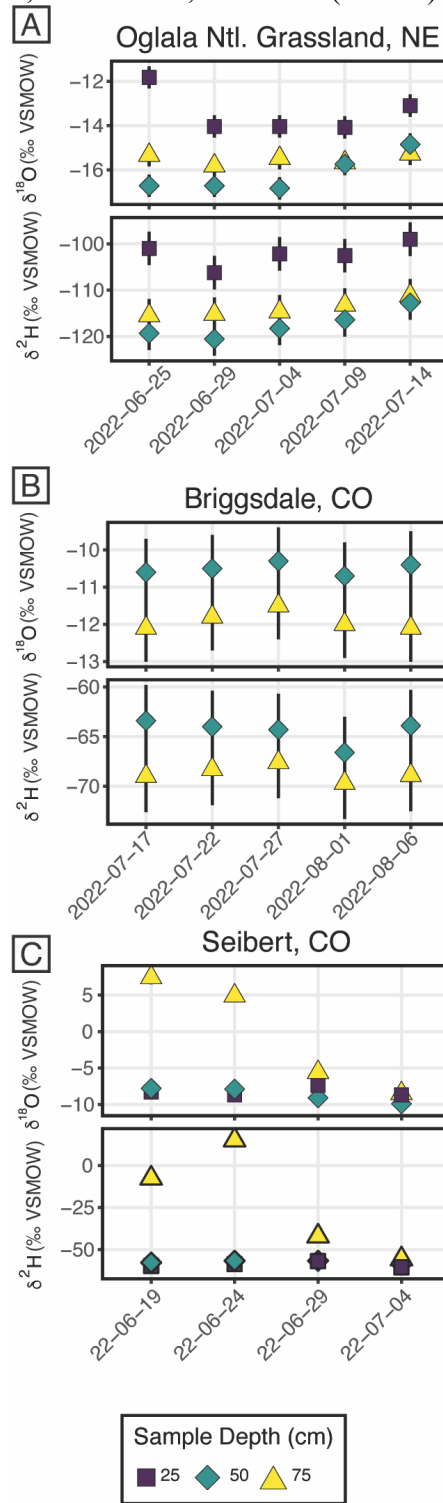
562



563  
 564 **Figure 6.** A) Results from three different field-based long dry air tests. B) Results from the automation  
 565 field suitability tests using the SWISS unit named Meringue. Flasks that sampled atmosphere are shown  
 566 in blue, flasks that sampled deionized water (DI) are shown in pink, and flasks that sampled the light  
 567 water are shown in yellow. The top plot shows the  $\delta^{18}\text{O}$  results, and the bottom plot shows the  $\delta^2\text{H}$  results.  
 568

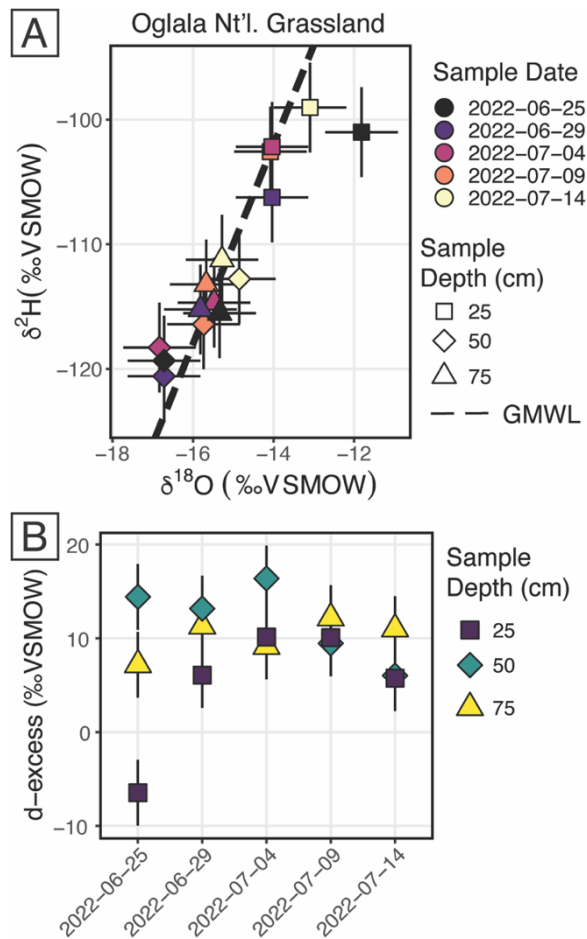
569 **5.3 Example Field deployment results**

570 Figure 7 shows the results from three field deployments in Oglala National Grassland,  
 571 Nebraska; Briggsdale, Colorado; and Seibert, Colorado (table 3).



572  
 573 **Figure 7.** Results from all three field deployments to A) Oglala National Grassland, NE, B) Briggsdale,  
 574 CO and C) Seibert, CO. Note, the y-axis scale for all three plots is different.

575 There are 15 samples from Oglala National Grassland (Fig. 7A, Table 3); five from 25  
 576 cm depth, five from 50 cm depth and five from 75 cm depth. Four of the five samples from 25  
 577 cm overlap within uncertainty in  $\delta^{18}\text{O}$  value, and all five samples overlap with uncertainty in  $\delta^2\text{H}$   
 578 value. There is a significant decrease in the  $\delta^{18}\text{O}$  value at 25 cm between 2022-06-25 and 2022-  
 579 06-29. There is no similar shift in  $\delta^2\text{H}$  value over the same time period. The first three samples  
 580 from 50 cm overlap in both  $\delta^{18}\text{O}$  and  $\delta^2\text{H}$  values, then the final two samples shift to higher  
 581 isotope values. Similar to the samples from 50 cm, there is a trend towards higher  $\delta^2\text{H}$  values for  
 582 the last three samples. All five samples from 75 cm overlap in  $\delta^{18}\text{O}$  and  $\delta^2\text{H}$  values. On a dual  
 583 isotope plot, data from 50 cm and 75 cm cluster together at lower values, while the  $\delta^{18}\text{O}$  and  $\delta^2\text{H}$   
 584 values from 25 cm are higher (Figs. 7A, 8A). All of the data overlap within uncertainty with the  
 585 global meteoric water line, except for the 25 cm depth sample from 2022-06-25 (Fig. 8A). The  
 586 calculated D-excess values are all within uncertainty of 10‰ and each other between 2022-06-29  
 587 and 2022-07-14 (Fig 8B), except for the 25 cm depth sample from 2022-06-25, which has a D-  
 588 excess value of -6.6‰, consistent with evaporative enrichment of soil water at that depth and  
 589 time.  
 590



591 **Figure 8.** Results from the Oglala National Grassland, NE field site. A)  $\delta^2\text{H}$  vs.  $\delta^{18}\text{O}$ , where the dashed  
 592 line is the global meteoric water line. The shapes for the different depths sampled matches figure 7, and  
 593 the color of the points is the date on which the soil water was sampled B) A plot of d-excess. Note, both  
 594 the color and shape match figure 7.  
 595

596           There are 10 samples from Briggsdale, CO (Fig. 7B, Table 3); five samples each from  
597 vapor probes buried at 50 cm and 75 cm depth. Data from 25 cm at Briggsdale, CO were  
598 excluded because the water vapor mole fractions from all of the flasks were extremely low  
599 (<13,000 ppm). We excluded these data because these samples are associated with a very dry  
600 soil (VWC < 0.05), and it is not clear how much sampling gas (N<sub>2</sub>) is injected into the soil using  
601 the vapor permeable tubing under very dry conditions (Quade et al., 2019), and therefore how  
602 representative these isotope data are of soil water. Moreover, below 13,000 ppm there are large  
603 linearity effects on a Picarro L2130-*i*, and it is challenging to correct those data if they were  
604 measured using the dry-air carrier sample introduction method. While all samples overlap within  
605 uncertainty for both  $\delta^{18}\text{O}$  and  $\delta^2\text{H}$  values, the absolute values of samples from 50 cm are  
606 consistently offset to higher values for both  $\delta^{18}\text{O}$  and  $\delta^2\text{H}$  as compared to samples from 75 cm.

607           There are 12 samples from Seibert, CO (Fig. 7C, Table 3); four from each sampling depth  
608 (25, 50 and 75 cm). At 25 cm depth,  $\delta^{18}\text{O}$  values of three of the four samples overlap within  
609 uncertainty, while the 25 cm sample from 2022-06-29 has a higher  $\delta^{18}\text{O}$  value than the other  
610 three samples. At 25 cm depth,  $\delta^2\text{H}$  values overlap within uncertainty for all four samples. At 50  
611 cm depth, there is a steady decrease in  $\delta^{18}\text{O}$  value over the sampling period, while  $\delta^2\text{H}$  values for  
612 all four samples remain steady and overlap within uncertainty. At 75 cm depth, samples have a  
613 very large range of  $\delta^{18}\text{O}$  values between -8.5‰ and 7.4‰, and  $\delta^2\text{H}$  values range between -  
614 55.7‰ and 15.1‰. Almost all of the samples from 75 cm depth were associated with  
615 condensation in the sample introduction lines during measurement.

**Table 3.** Results from the three field deployments of SWISS.

Site	Date	Sample Depth (cm)	Flask	T (°C)	$\delta^{18}\text{O}$ (‰)	$\delta^{18}\text{O}$ (‰) Analytical Error	$\delta^2\text{H}$ (‰)	$\delta^2\text{H}$ (‰) Analytical Error
Briggsdale	2022-07-17	50	3	25.1	-10.8	0.2	-65.6	0.6
Briggsdale	2022-07-17	75	4	23	-12.1	0.2	-69	0.7
Briggsdale	2022-07-22	50	6	25.9	-10.7	0.3	-67.1	0.7
Briggsdale	2022-07-22	75	7	23.6	-11.9	0.2	-69	0.6
Briggsdale	2022-07-27	50	9	24.3	-10.4	0.3	-65.6	0.6
Briggsdale	2022-07-27	75	10	23	-11.5	0.2	-67.6	0.7
Briggsdale	2022-08-01	50	12	23.4	-10.7	0.2	-67	0.7
Briggsdale	2022-08-01	75	13	22.4	-12.0	0.2	-69.1	0.7
Briggsdale	2022-08-06	50	15	24	-10.5	0.2	-65	0.6
Briggsdale	2022-08-06	75	16	22.9	-12.1	0.2	-68.8	0.7
Seibert	2022-06-19	25	2	24.2	-8.3	0.2	-59.8	0.6
Seibert	2022-06-19	50	3	22	-7.8	0.2	-57.8	0.6
Seibert	2022-06-19	75	4	19.4	7.4	0.2	-7.6	0.7
Seibert	2022-06-24	25	5	24	-8.7	0.2	-58.7	0.7
Seibert	2022-06-24	50	6	22.2	-7.9	0.2	-56.7	0.7
Seibert	2022-06-24	75	7	20.5	4.9	0.2	15.1	0.6
Seibert	2022-06-29	25	8	23.2	-7.4	0.2	-56.9	0.6
Seibert	2022-06-29	50	9	21.8	-9.1	0.2	-56.7	0.7
Seibert	2022-06-29	75	10	21	-5.6	0.2	-42.1	0.6
Seibert	2022-07-04	25	11	25	-8.7	0.2	-60.6	0.7
Seibert	2022-07-04	50	12	23.3	-9.9	0.2	-58.8	0.6
Seibert	2022-07-04	75	13	21.5	-8.5	0.2	-55.7	0.7
Oglala Ntl. Grassland	2022-06-25	25	2	23.0	-11.8	0.2	-101	0.7
Oglala Ntl. Grassland	2022-06-25	50	3	22.8	-16.7	0.2	-119.3	0.7
Oglala Ntl. Grassland	2022-06-25	75	4	21.5	-15.3	0.2	-115.5	0.8
Oglala Ntl. Grassland	2022-06-29	25	5	25.0	-14	0.2	-106.2	0.7
Oglala Ntl. Grassland	2022-06-29	50	6	22.8	-16.7	0.2	-120.6	0.7
Oglala Ntl. Grassland	2022-06-29	75	7	21.3	-15.8	0.2	-115.2	0.7
Oglala Ntl. Grassland	2022-07-04	25	8	25.0	-14	0.2	-102.2	0.7
Oglala Ntl. Grassland	2022-07-04	50	9	23.0	-16.8	0.2	-118.3	0.6
Oglala Ntl. Grassland	2022-07-04	75	10	22.0	-15.5	0.2	-114.7	0.6
Oglala Ntl. Grassland	2022-07-09	25	11	23.0	-14.1	0.2	-102.6	0.6
Oglala Ntl. Grassland	2022-07-09	50	12	22.8	-15.7	0.2	-116.4	0.7
Oglala Ntl. Grassland	2022-07-09	75	13	22.0	-15.7	0.2	-113.2	0.6
Oglala Ntl. Grassland	2022-07-14	25	14	23.0	-13.1	0.2	-99	0.6
Oglala Ntl. Grassland	2022-07-14	50	15	22.8	-14.9	0.3	-112.8	0.7
Oglala Ntl. Grassland	2022-07-14	75	16	22.0	-15.3	0.2	-111.2	0.7

619 **6. Discussion**

620 **6.1 QA/QC and field suitability tests**

621 **6.1.1 Dry Air tests**

622 In Colorado, where these tests were completed, the ambient atmosphere during the  
623 summertime typically sits at a water vapor mole fraction between 10,000 - 20,000 ppm, and in  
624 winter the water vapor mole fraction can drop as low as 4000 ppm. If the flasks had been slowly  
625 equilibrating with the atmosphere, the flasks would have drifted to much higher water vapor  
626 molar fractions. If the flasks did not drift towards higher water vapor mole fractions, we felt  
627 confident that the flasks are resistant to atmospheric intrusion after they have been flushed with  
628 dry air. We chose a timescale of seven days for the dry air tests because we found that in a low-  
629 humidity environment, seven days was enough time to meaningfully observe leaks, while being  
630 short enough to work through the QA/QC process efficiently. For example, results of two  
631 sequential dry air tests on the SWISS unit Toblerone (supplemental Fig. 2), show that it is  
632 possible to drastically reduce leaks that allow ambient water vapor in the air from intruding into  
633 the flasks by tightening and/or replacing problematic fittings (both those attached to the glass  
634 flasks and those on the Valco valve) and in some cases the glass flask itself. During the final  
635 seven-day dry air tests, most flasks maintained a water vapor mole fraction less than 400 ppm,  
636 and all flasks maintained a water vapor mole fraction of less than 700 ppm (Fig. 3).

637 Across all of the SWISS units, there is a bias towards a higher water vapor mole fraction  
638 for the first flask that is measured (port one on every valve is the flask bypass loop, so the first  
639 flask is flask two), which suggests a methodological source of higher water vapor concentration  
640 rather than Swagelok fitting tightness problems. There are two potential sources for this issue.  
641 First, it is possible that not all of the atmospheric water vapor was flushed from the line that  
642 connects to the CRDS prior to the start of the measurements, but by the time the second flask is  
643 measured, the lines between the SWISS and CRDS have been sufficiently flushed, creating bias  
644 in the first flask measured. This hypothesis could be tested by flushing all of the gas lines with  
645 dry air to progressively lower water vapor mixing ratios prior to measuring any flasks, to see  
646 what minimum ratio is required to eliminate this bias. Lab protocols can then be adjusted to flush  
647 all gas lines to this level. Similarly, it is possible that during the filling phase, not all of the  
648 atmospheric vapor has been flushed out of the Drierite system before starting the fill process.  
649 This hypothesis is supported by the systematic decrease in water vapor mole fraction across  
650 flasks in the Toblerone unit (Fig. 3, right panel). As a result of these biases, we now flush the  
651 Drierite for at minimum 30 minutes prior to the start of the experiment.

652 In addition to testing the leakiness, the dry air test also provided a useful baseline from  
653 which to test building materials. For example, in supplemental figure 5, we show the results of  
654 sequential seven day and 27-day dry air tests where we replaced stainless steel tubing and fittings  
655 with PTFE Swagelok fittings with 1/8 inch PTFE tubing. We thought that PTFE fittings would  
656 be advantageous because they are much easier to install and are significantly lighter, and would  
657 therefore be helpful when there are weight constraints. However, based on the very limited  
658 testing we did, PTFE fittings and tubing *may be* sufficient to store water for up to a single week,  
659 but on longer timescales (e.g. 27 days) we observed greater exchange and leaking than with the  
660 stainless steel fittings. We encourage any future user using this modification to rigorously test  
661 these fittings on a timescale appropriate for their application.

662



### 663 6.1.2 Water vapor tests

664 Our initial goal with the water vapor tests was to test whether the measured water vapor  
665 isotope values at the end of the two-week holding period were normally distributed about 0  
666 within the uncertainty limits of the water vapor probes (Oerter et al., 2016). This was a  
667 reasonable goal given the similarities in probe set-up and the plumbing design between the  
668 SWISS and the IsoWagon system. But, the most salient result of the water vapor tests is that  
669 there is a consistent positive offset between the input isotope values and the isotope values  
670 measured at the end of the two-week experiments (Figs 4B, 5B). The positive offset in both  $\delta^{18}\text{O}$   
671 and  $\delta^2\text{H}$  values is consistent across 11 different tests, using six different SWISS and three  
672 different input water isotope values. If there was alteration of original values due to leaky flasks,  
673 we might expect the  $\delta^{18}\text{O}$  and  $\delta^2\text{H}$  values to converge on the  $\delta^{18}\text{O}$  and  $\delta^2\text{H}$  value of the  
674 atmosphere. For example, we might expect water vapor from the light water test to have the most  
675 significant change in isotope value, towards that of the ambient atmosphere. Instead, the  
676 consistency across >135 flasks, different starting water vapor isotope values, sample introduction  
677 methods, and multiple analytical sessions suggests that this difference is a function of the storage  
678 and measurement process. In particular, the normality of the distribution suggests whatever the  
679 origin of the offset is, there is a systematic bias that we can reliably correct for.

#### 680 6.1.2.1 Offset correction

681 To correct our data for this offset, we chose to use the median value as an offset  
682 correction rather than the mean of the normal distribution, because the median is not biased by  
683 major outlier isotope values that reflect abnormal values that go beyond analytical noise, such as  
684 a slow but major leak that changes the values far beyond the basic offset seen in the dataset. The  
685 calculated average offset is 1.0‰ and 2.6‰ for  $\delta^{18}\text{O}$  and  $\delta^2\text{H}$ , respectively. After applying these  
686 values as an offset correction to the data, most flasks also fall within the uncertainty of the water  
687 vapor permeable probes ( $\delta^{18}\text{O} = \pm 0.5\text{‰}$  and  $\delta^2\text{H} = \pm 2.4\text{‰}$ , Oerter et al., 2016), and the values  
688 are distributed about 0 (Figs. 4C, 5C). However, the uncertainty of the SWISS system is higher  
689 than that of the probes alone. Based on the results of the water vapor tests, we estimate the  
690 uncertainty of the SWISS at  $\pm 0.9\text{‰}$  and  $\pm 3.7\text{‰}$  for  $\delta^{18}\text{O}$  and  $\delta^2\text{H}$ , respectively using the  
691 interquartile range (IQR) of the water vapor test results after removing outliers from the dataset.  
692 We prefer the IQR over the calculated standard deviation of the normal distribution, because  
693 IQR is not biased by outlier values. This level of uncertainty is large relative to other methods,  
694 but is sufficient for many critical zone applications, given the magnitude of seasonal variability  
695 in the top ~50 cm of a soil profile that can be observed in natural systems (e.g. Oerter et al.,  
696 2017; Quade et al., 2019). We also expect that uncertainties will decrease with future lab-based  
697 or near research facility testing and by comparing the SWISS against other soil water extraction  
698 methods.

700 The relationship between  $\delta^2\text{H}$  values and  $\delta^{18}\text{O}$  values in a dual-isotope plot provides  
701 insight into the mechanism driving the offset. Without an offset correction applied, the slope of  
702 the relationship between  $\delta^2\text{H}$  and  $\delta^{18}\text{O}$  is 3.14 ( $R^2 = 0.62$ ) (Supplemental Fig. 4). This slope is  
703 only slightly higher than evaporation under pure diffusion (Gonfiantini et al., 2018). This  
704 suggests that the offset is likely driven by diffusion and will likely vary according to climate of  
705 the lab. For example, in a dry climate like Colorado, the water vapor concentration in the flask is  
706 significantly higher than the atmosphere, creating a larger diffusive gradient potential than for a  
707 lab in a more humid climate. We therefore strongly encourage future users to test their SWISS under  
708 climate conditions similar for their applications. Further, we encourage users who might use the

709 SWISS as part of a tracer study that uses labeled heavy water to test the SWISS with labeled  
710 waters prior to their field experiments to verify reliability.

711

#### 712 *6.1.2.2 Comparing sample introduction methods*

713 Supplemental figure 6 shows a kernel density estimate plot of the results from two water  
714 vapor test sessions, with the offset correction applied. During the March 2022 session, flasks  
715 were measured using the dead-end pull sample introduction method and during the August 2022  
716 session, flasks were measured using the dry air carrier gas sample introduction method. There is  
717 no significant difference in the measured difference between the two sample introduction  
718 methods. That said, we prefer the dry air carrier gas method, because it is far simpler to control  
719 the water vapor mixing ratio, and optimize the concentration to be around 25,000 ppm, which is  
720 the concentration at which the Picarro L2130-*i* is most reliable. The dry air carrier gas method  
721 also makes it easier to control for and monitor for condensation in the stainless-steel tubing and  
722 vapor impermeable tubing, which can bias a measurement.

723

#### 724 *6.1.3 Field suitability tests*

725 The long dry air tests in the field are a useful complement to the shorter in-lab tests  
726 because they test the reliability of the system at field-deployment timescales. It is clear from the  
727 34 and 43 day tests that the flasks are reasonably resistant to leaks on the timescale of a normal 4  
728 – 6 week deployment (Fig. 6A). These tests also give us confidence that flasks filled later in the  
729 sampling sequence do not take on an atmospheric signal prior to sampling. There are a few  
730 possibilities to explain the poorer performance of the Toblerone SWISS unit during the 52-day  
731 test. (Fig. 6A). The first is that there is a real threshold past which the SWISS are no longer able  
732 to retain samples. However, this explanation would suggest that there should be a gradual  
733 decrease in performance across the three tests, which we do not observe. The alternative  
734 explanation is that the poor performance is a result of inter-unit variability. The 52-day test was  
735 the first long-term test and was performed in August 2021. In August 2021, we were continuing  
736 to build new SWISS units and continuing to learn from each successive round of QA/QC, so it  
737 seems plausible that there were unidentified problems with the SWISS unit Toblerone that were  
738 solved before the water vapor tests in August 2022.

739 In figure 6B, the data show that the flasks preserved the  $\delta^{18}\text{O}$  value of both flash-  
740 evaporated and atmospheric water vapor over a seven-day period. One flask was removed from  
741 the dataset (flask eight), because there was visible condensation in the clear impermeable tubing  
742 during the measurement phase, with an increase of  $> 5\%$  for  $\delta^{18}\text{O}$  during the measurement  
743 period. The condensation appeared as small ( $<1$  mm) bubbles of water all along the impermeable  
744 tubing, but the bubbles were concentrated near the connection between the SWISS and the  
745 impermeable tubing. Notably, the two flasks whose  $\delta^{18}\text{O}$  values do not overlap within  
746 uncertainty are more negative than expected, rather than drifting towards atmospheric values or  
747 values expected from diffusive fractionation. In contrast to the  $\delta^{18}\text{O}$  values, only 3 flasks filled  
748 with flash evaporated water vapor overlap within uncertainty of the known  $\delta^2\text{H}$  values, while  
749 four of the five flasks overlap within uncertainty of the estimated atmosphere isotope value. The  
750 flasks tend to drift towards the value of the atmosphere, but retain the overall data pattern from  
751 the oxygen isotope values.

752 The relatively high failure rate of this ‘mock’ field test was somewhat surprising given  
753 the results of the water vapor tests done in the laboratory. Going into the test, we suspected that  
754 flasks six and eight were slightly leaky based on previous water vapor tests; these were flasks

755 that previously performed poorly, but did not ‘fail’ during the water vapor test. Once we  
756 collected the data, we compared the data for flasks six and eight to other flasks in the sequence.  
757 During the measurement of flask eight, we observed condensation in the sample introduction  
758 lines, and because the isotope values were so different relative to other flasks, we felt confident  
759 in our exclusion of flask eight. Flask six had  $\delta^{18}\text{O}$  and  $\delta^2\text{H}$  values similar to others from the  
760 same sampling source, and seemed to fall within the pattern as expected. Therefore, we chose to  
761 keep this data point in the dataset.

762 We hypothesize that one major problem with the mock field test dataset was the creation  
763 of condensation in the sampling lines, as others have experienced in their setups (e.g. Quade et  
764 al., 2019; Kühnhammer et al., 2019). Of particular interest are the flasks that had a lower than  
765 expected  $\delta^{18}\text{O}$  value (flasks four and nine). It is possible that those samples were also affected by  
766 condensation, but in contrast to flask eight, which was excluded because of condensation during  
767 measurement, we think that these samples may have been altered because of condensation at the  
768 sampling stage. During condensation, we expect that  $^{18}\text{O}$  will preferentially enter the liquid  
769 phase, and that the water vapor that enters the flask will have a lower than expected  $\delta^{18}\text{O}$  value.  
770 The unique advantage of the SWISS is that it can operate independently, but with that comes the  
771 trade-off that we cannot currently observe condensation in the lines during sample collection. To  
772 prevent condensation from forming, other users have warmed the impermeable tubing between  
773 the probes and the Picarro. The ‘mock’ field test data suggest that in many situations it may be  
774 worthwhile to warm the transfer tubing, but this should be done in a way that does not alter the  
775 thermal structure of the soil, and in remote settings, can operate safely independently.

#### 776 777 ***6.1.4 Lessons learned and recommendations from the QA/QC and field suitability tests:***

778 Our QA/QC process was a relatively efficient way to test the soundness of the SWISS  
779 units. Through the QA/QC process we were able to identify problems with units, and  
780 appropriately address them before deploying units to the field. We strongly recommend that any  
781 user deploying SWISS to the field to undertake the same, or similar, QA/QC process.

782 The dry air test is a time-efficient and low-cost method for identifying flasks that are  
783 leaky and will not preserve the sampled water vapor isotope values. It is useful during the  
784 building stage to identify fittings that need to be tightened or flasks that need to be replaced, and  
785 therefore we recommend these tests as a required pre-deployment step for future SWISS units.  
786 We found that it was most time and energy efficient to move onto the next level of QA/QC once  
787 13 out of 15 flasks of a SWISS unit had passed the dry-air test, because frequently the remaining  
788 two flasks still had relatively low water vapor mole fractions (i.e. 500 – 700 ppm), and we could  
789 sufficiently tighten the fittings prior to the start of the water vapor tests for them to be successful.  
790 The dry air test is a low time and expense burden that can also be used to monitor SWISS units  
791 for normal wear-and-tear (e.g. a flask that cracked during transport) during deployment periods.  
792 Therefore, to ensure that SWISS units continue to operate as expected, we also recommend that  
793 dry air tests be done between field deployments on every SWISS unit. Lastly, we note that the  
794 dry air test could be modified based on available equipment (for example, if an instrument is  
795 available to measure trace atmospheric gases, that could be used instead).

796 Based on the results of the long, field dry air test, we recommend that the water vapor  
797 storage time doesn’t exceed 40 days for reliable results, or that the user undertake multiple dry  
798 air tests with either lower concentration benchmarks or longer duration if deployments may  
799 exceed 40 days.

800 Overall, the quality control and quality assurance as well as the field suitability tests  
801 demonstrate that the SWISS units can retain the isotope values of water vapor collected using  
802 water vapor permeable probes. Like many other systems that measure dual isotopes, each system  
803 (i.e.  $\delta^{18}\text{O}$  and  $\delta^2\text{H}$ ) must be evaluated separately. In general, we interpret oxygen isotope data  
804 with a higher degree of confidence than the hydrogen isotope data. As the automation test  
805 revealed however, even when the absolute  $\delta^2\text{H}$  value is not correct, the general pattern can reveal  
806 information about soil water dynamics.

807 Finally, we opted to use a large flask volume because it allows us to measure a sample for  
808 long enough on a CRDS that we get reliable data, without interacting with vapor bound to the  
809 flask walls. The drawback of this, however, is that we must sample soil water vapor for a  
810 relatively long period of time (45 minutes). In supplemental figure 7, we show that the sampling  
811 regime, and particularly the length of time we pump dry air through the tubing, does not  
812 significantly alter the soil moisture content of the soil. Additionally, we demonstrate that the  
813 sampling regime we use does not introduce significant memory effects.

814

## 815 **6.2 Field Deployments**

816 In Figure 7 we show the results of three field deployments completed during summer  
817 2022 (Table 3). At the Oglala National Grassland site, we used the SWISS unit named Lindt to  
818 collect samples. During the August 2022 water vapor test on Lindt, all  $\delta^{18}\text{O}$  values fall within  
819 uncertainty of the system, and nine of the fifteen  $\delta^2\text{H}$  values fall within uncertainty of the  
820 system. Therefore, we interpret the  $\delta^{18}\text{O}$  values with greater confidence and the  $\delta^2\text{H}$  values with  
821 lower confidence (Figs. 4C and 5C). We note that the  $\delta^{18}\text{O}$  and  $\delta^2\text{H}$  values broadly follow the  
822 same trends, and fall on the global meteoric water line (Figs. 7 and 8A). In general, soil water  
823 from 25 cm had higher  $\delta^{18}\text{O}$  and  $\delta^2\text{H}$  values than soil water from both 50 and 75 cm (Fig. 8A).  
824 Given that 4 of the 5 samples from 25 cm overlap with the GMWL and have a d-excess that  
825 overlaps with  $10 \pm 2.6\text{‰}$ , the soil water from that depth may reflect summer precipitation with  
826 higher  $\delta^{18}\text{O}$  and  $\delta^2\text{H}$  values. Soil water from 75 cm had intermediate  $\delta^{18}\text{O}$  and  $\delta^2\text{H}$  values for  
827 most of the study period, and soil water from 50 cm depth had the lowest  $\delta^{18}\text{O}$  and  $\delta^2\text{H}$  values  
828 for most of the study period, which may reflect a more mean-annual or winter precipitation  
829 biased value. Based on data available from the National Weather Service (Chadron, NE), there  
830 were likely significant precipitation events on 2022-06-25 and 2022-07-08 at the field site. There  
831 is a significant shift to lower  $\delta^{18}\text{O}$  values at a sampling depth of 25 cm between 2022-06-25 and  
832 2022-06-29, as well as a marked increase in the d-excess value (Fig. 8A). We interpret this shift  
833 as infiltration of precipitation with lower  $\delta^{18}\text{O}$  values, which is supported by a return of d-excess  
834 values to  $\sim 10\text{‰}$  (Fig. 8A). The National Weather Service reported 21.33 mm (0.84 inches) of  
835 rain at Chadron Municipal Airport, approximately 50 km from the study site on 2022-07-08,  
836 which likely was associated with at least some precipitation at our field site. Following the  
837 significant rain event on 2022-07-08, we observe a marked increase in the stable isotope value of  
838 water vapor from a sampling depth of 50 cm, towards values that are much closer to those at 25  
839 cm depth. These data suggests that soil water isotopes at 50 cm in this silt-loam Aridisol may be  
840 fairly sensitive to large individual precipitation events, while at 75 cm soil water isotopes remain  
841 comparatively uniform. Future work should address how drought conditions, storm size, pore  
842 size distribution, and soil clay mineralogy influence the variability of soil water isotopes with  
843 depth.

844 At Briggsdale, CO we used the SWISS named Raclette to collect soil water vapor  
845 samples. Data from 25 cm depth at Briggsdale, CO were discarded because the water vapor mole

846 fraction was much lower than would be expected given the soil temperature (i.e. < 15,000 ppm).  
847 The gravimetric water concentration (GWC) at that soil depth at the time of sampling was  
848 approximately 4% through the sampling period. Future work should include a multiple-method  
849 (e.g. cryogenic extraction, centrifugation, etc.) comparison of soil water isotopes at low water  
850 contents to better understand what these samples might represent, and if they are actually  
851 representative of soil conditions.

852 Based on the results of the August 2022 water vapor test done on Raclette where all  
853 flasks fell within uncertainty of the SWISS system for both  $\delta^{18}\text{O}$  and  $\delta^2\text{H}$ , except for flask 11  
854 (Figs. 4C and 5C), we interpret all data with greater confidence. Flask 11 corresponds to the 25  
855 cm depth sample from 2022-07-27, and was already culled from the dataset because of low water  
856 vapor mole fraction associated with the very dry soil. The soil water  $\delta^{18}\text{O}$  and  $\delta^2\text{H}$  values from a  
857 sampling depth of 50 cm and 75 cm overlap within uncertainty, but the soil water  $\delta^{18}\text{O}$  and  $\delta^2\text{H}$   
858 values from 50 cm are higher than the isotope values from 75 cm. All of the data from each  
859 sampling depth group (i.e. 50 cm and 75 cm) overlap within uncertainty, conforming to the  
860 expectation that soil water from these sampling depths should be fairly invariant (e.g. Oerter et  
861 al., 2019). There were precipitation events at the study site on 2022-07-24, 2022-07-28 and  
862 2022-07-31. It is possible that the slight negative shift in both  $\delta^{18}\text{O}$  and  $\delta^2\text{H}$  on 2022-08-01  
863 reflects infiltration of precipitation to those depths, but this is not certain given that all of the  
864 measurements from within a sampling depth overlap within uncertainty.

865 At Seibert, CO we used the SWISS named Toblerone to collect soil water vapor samples.  
866 The soil water isotope data from 75 cm depth at this site offer a few useful lessons for future  
867 users. The two key observations of the data from 75 cm depth are that the  $\delta^{18}\text{O}$  and  $\delta^2\text{H}$  values  
868 are much higher than the other two sampling depths, and that the  $\delta^2\text{H}$  and  $\delta^{18}\text{O}$  values do not  
869 move in parallel with each other. While measuring these samples we observed condensation in  
870 the impermeable tubing at the point where the SWISS connects to the impermeable tubing.  
871 Additionally, when we heated the stainless steel tubing that connects the tubing flask and Valco  
872 valve we observed a rapid increase in water vapor mole fraction (1000's of ppm over <30  
873 seconds) that was accompanied by a rise in stable isotope value. During these measurements, we  
874 were rarely able to get a stable isotope value measurement window, and instead the stable  
875 isotope value of the vapor increased continually through the measurement. It is for these reasons  
876 that we feel confident in discarding the stable isotope data from 2022-06-19 – 2022-06-29. The  
877 final measurement from 75 cm depth on 2022-07-04 approaches a reasonable isotope value when  
878 compared to isotope values from the other two depths, and that sample had fewer condensation  
879 problems during measurement. However, because we have no sequential context for what a  
880 reasonable value for this depth is, we discarded that value as well. For that final 75 cm sample,  
881 we were more successful because we warmed the entire length the vapor impermeable tubing, as  
882 well as the stainless-steel tubing, flask, and Valco valve evenly so that there were no temperature  
883 gradients across the vapor path. If the condensation had only been in the impermeable tubing it  
884 would have been much easier to successfully analyze these samples by just closing off the flask  
885 and running dry air through the tubing to remove condensation, but because condensation was  
886 also occurring in the stainless steel tubing between the flask and Valco valve, this was not  
887 possible. It remains unclear why condensation was such a significant problem for samples from  
888 that depth as opposed to samples from different depths in the same SWISS. Future work should  
889 include further testing of the SWISS across different water contents and temperatures to better  
890 understand why the phenomenon may have occurred.

891 Based on the results of the August 2022 water vapor test done on Toblerone, we interpret  
892 all data from 50 cm and 25 cm depth with high confidence, except for Flask 3, which is the 50  
893 cm sample from 2022-06-19 (Figs. 4C and 5C). Unlike data from the other two field sites, soil  
894 water from 25 cm and 50 cm overlap within uncertainty. There were two precipitation events at  
895 the field site during the sampling period on 2022-06-25 and 2022-07-01, but both events were  
896 quite small (<0.5 mm, CoAgMet). There is no significant influence of the precipitation events on  
897 the  $\delta^{18}\text{O}$  and  $\delta^2\text{H}$  values. The >1.0‰ increase in  $\delta^{18}\text{O}$  values on 2022-06-29 is surprising given  
898 that there is not a comparable magnitude increase in  $\delta^2\text{H}$  value, and that the values measured  
899 from 2022-07-04 more closely match the  $\delta^{18}\text{O}$  and  $\delta^2\text{H}$  values from the two earlier sampling  
900 days. There are two potential explanations for this data. First, that this shift is a real signal from  
901 an evaporation driven increase in the  $\delta^{18}\text{O}$  value, and the shift back to a lower  $\delta^{18}\text{O}$  value on  
902 2022-07-04 is due to the infiltration of precipitation, which could also explain the low d-excess  
903 value associated with this measurement (Supplemental Fig. 8 ). The second possible explanation  
904 is that the 25 cm sample from 2022-06-29 is influenced by condensation at the time of sampling.  
905 Dew point at the field site on 2022-06-29 significantly decreased as compared to the other  
906 sampling days to a monthly minimum of 20.6°C (CoAgMet). It is possible that environmental  
907 conditions encouraged the formation of condensation in the impermeable tubing at the time of  
908 sampling. There were no obvious signs of condensation during the time of measurement in the  
909 lab. These results highlight the utility of having broad contextual environmental data to aid in the  
910 interpretation of soil water isotope data.

911 All together, these three soil water isotope datasets demonstrate two main findings. First,  
912 data from these samples show that the differences between field sites are easily resolvable using  
913 the SWISS. For example, at 50 cm depth the oxygen isotopes range between -14.4 to -16.3‰, -  
914 9.9 to -10.3‰, and -7.4 to -9.3‰ for the Oglala, Briggsdale and Seibert sites, respectively. These  
915 differences likely reflect differences in the stable isotope composition of precipitation and  
916 infiltration and evaporation dynamics. Second, the sample data retrieved from a SWISS are  
917 sufficiently precise to be able to meaningfully resolve vertical profile soil water isotope data. For  
918 example, at the Oglala National Grassland field site, soil water from 25 cm clearly has higher  
919  $\delta^{18}\text{O}$  and  $\delta^2\text{H}$  values as compared to soil water from a depth of 50 and 75 cm.

920

### 921 **6. 3 Future improvements and future work**

922 One significant SWISS unit hardware improvement that could be made would be to  
923 install a heating implement to the flasks. One source of uncertainty on the current system is the  
924 potential effect of uneven heating of the flasks prior to measurement which may create  
925 temperature gradients that are large enough to allow for condensation when warm vapor meets a  
926 slightly colder spot. This could be improved in subsequent iterations of the SWISS with the  
927 addition of heat tape or blankets that can deliver controlled heat and create consistent  
928 temperatures. This improvement would also help limit the amount of manual intervention needed  
929 during measurement, and could improve automation of flask measurement. Additionally, finding  
930 a way to safely and automatically heat the impermeable tubing that connects the water vapor  
931 probes and the SWISS in a way that doesn't change the inherent thermal structure of the soil, and  
932 is safe for unmonitored use, would help to prevent the formation of condensation in the field and  
933 reduce the uncertainties related to sampling.

934 We have made a few improvements to the automation system that were not implemented  
935 for the data presented in this contribution, but will be part of future deployments. First, we will  
936 track conditions inside the SWISS with a temperature and relative humidity sensor inside the

937 case. Second, we plan to eliminate the power inverter by powering both the Valco valve and  
938 mass flow controller with VDC using a power step up controller. Lastly, we will add an IoT  
939 cellular router to be able to remotely monitor and control the SWISS units. This would be  
940 particularly helpful if there is a sampling day that is unexpectedly cold or when the dew point at  
941 the field site is unexpectedly low and we expect condensation to form more readily in the  
942 field, or if there is a precipitation event that we are interested in capturing, because with the IoT  
943 cellular router we could remotely alter the sampling plan.

944 While the improvements and additional testing we have done to the SWISS in this  
945 contribution represent a significant step forward, additional work should be done to make the  
946 system more useable by the ecohydrology community. We have rigorously tested the SWISS in  
947 the lab, and demonstrated a few ways in which the SWISS can fail in field settings. A full  
948 comparison of how soil water isotope data collected using a SWISS as compared to other in situ  
949 (both vapor probes and lysimeter) and destructive sampling methods would shed light on the  
950 accuracy and precision of our system, and the applicability of our lab-based experiments to the  
951 field. These experiments should be carefully designed with considerations of soil grain size, soil  
952 water content, expected isotope values, and climate. Additionally, we plan to test SWISS unit  
953 resilience during air travel so that these units can be used at field sites that are not within driving  
954 distance of a research facility.

## 955 **Conclusions**

956 We presented the evolution of the soil water isotope storage system (SWISS) from a  
957 prototype to a fully built out and tested system. We also presented a quality control and quality  
958 assurance procedure that we strongly recommend future users undertake to ensure the reliable  
959 storage of soil water vapor over long time periods (up to 40 days). In addition, these quality  
960 control and quality assurance tests shed light on the accuracy and precision of the SWISS. After  
961 applying an offset correction, we determine the precision of the SWISS to be  $\pm 0.9\%$  and  $\pm 3.7\%$   
962 for  $\delta^{18}\text{O}$  and  $\delta^2\text{H}$ , respectively. In a field setting, flasks reliably resist atmospheric intrusion.  
963 Additionally, the proposed sampling schema does not introduce significant memory effects.  
964 Lastly, we demonstrate that the current precision of the SWISS still allows us to distinguish  
965 between field sites and between soil water dynamics within a single soil column. Taken as a  
966 whole, these data show that the SWISS can be used as a tool to answer many emerging  
967 ecohydrological questions, and will enhance researchers' ability to collect soil water isotope  
968 datasets from more remote and traditionally understudied field sites.

## 969 **Acknowledgements**

970 We thank the numerous field assistants who helped to make the field work presented in  
971 this paper possible, including Spencer Burns, Anne Fetrow, Sarah Brookins, Juliana Olsen-  
972 Valdez, and Haley Brumberger. We acknowledge that both field work and laboratory work for  
973 this study were done on the traditional territories and ancestral homelands of the Arapahoe, Ute  
974 and Cheyenne peoples. This work was supported by startup funding from CU Boulder and NSF  
975 funding from grant EAR-2023385 awarded to K. Snell. Additionally, this work was supported by  
976 the University of Colorado Boulder Beverly Sears Research Grant and the Clay Minerals Society  
977 Graduate Student Research Grant both awarded to R. Havranek. CUBES-SIL is a CU Boulder  
978 Core Facility associated with RRID: SCR\_019300.

979

980 **Author contribution**

981 Rachel E. Havranek: conceptualization, methodology, investigation, formal analysis, funding

982 acquisition, writing – wrote original draft, review and editing. Kathryn E. Snell:

983 conceptualization, methodology, writing – review & editing, funding acquisition. Sebastian H.

984 Kopf: conceptualization, methodology, writing – review & editing. Brett Davidheiser-Kroll:

985 conceptualization, methodology, writing – review & editing. Valerie Morris: methodology,

986 writing – review & editing. Bruce Vaugh: methodology, writing – review & editing.

987

988 **Competing interests**

989 The authors declare no competing interests.



## 990 Works Cited

- 991 Beyer, M., Kühnhammer, K., & Dubbert, M. (2020). In situ measurements of soil and plant  
992 water isotopes : a review of approaches , practical considerations and a vision for the future.  
993 *Hydrology and Earth System Sciences*, 24, 4413–4440.  
994 <https://doi.org/https://doi.org/10.5194/hess-24-4413-2020>
- 995 Bowen, G. J., Cai, Z., Fiorella, R. P., & Putman, A. L. (2019). Isotopes in the Water Cycle:  
996 Regional- to Global-Scale Patterns and Applications. *Annual Review of Earth and Planetary*  
997 *Sciences*, 47(1), 453–479. <https://doi.org/10.1146/annurev-earth-053018-060220>
- 998 Bowen, G. J., Putman, A., Brooks, J. R., Bowling, D. R., Oerter, E. J., & Good, S. P. (2018).  
999 Inferring the source of evaporated waters using stable H and O isotopes. *Oecologia*, 187(4),  
1000 1025–1039. <https://doi.org/10.1007/s00442-018-4192-5>
- 1001 Brooks, J. R., Barnard, H. R., Coulombe, R., & McDonnell, J. J. (2010). Ecohydrologic  
1002 separation of water between trees and streams in a Mediterranean climate. *Nature*  
1003 *Geoscience*, 3(2), 100–104. <https://doi.org/10.1038/ngeo722>
- 1004 CoAgMet, Colorado Climate Center, Colorado State University, Fort Collins, CO, USA.  
1005 <https://coagmet.colostate.edu/>
- 1006 Dawson, T. E., & Ehleringer, J. R. (1991). Streamside trees that do not use stream-water:  
1007 evidence from hydrogen isotopes ratios. *Nature*, 350(March), 335–337.
- 1008 Gaj, M., Beyer, M., Koeniger, P., Wanke, H., Hamutoko, J., & Himmelsbach, T. (2015). In-situ  
1009 unsaturated zone stable water isotope (2H and 18O) measurements in semi-arid  
1010 environments using tunable off-axis integrated cavity output spectroscopy. *Hydrology and*  
1011 *Earth System Sciences Discussions*, 12(6), 6115–6149. [https://doi.org/10.5194/hessd-12-](https://doi.org/10.5194/hessd-12-6115-2015)  
1012 [6115-2015](https://doi.org/10.5194/hessd-12-6115-2015)
- 1013 Gaj, M., Beyer, M., Koeniger, P., Wanke, H., Hamutoko, J., & Himmelsbach, T. (2016). In situ  
1014 unsaturated zone water stable isotope (2H and 18O) measurements in semi-arid  
1015 environments: A soil water balance. *Hydrology and Earth System Sciences*, 20(2), 715–731.  
1016 <https://doi.org/10.5194/hess-20-715-2016>
- 1017 Gessler, A., Bächli, L., Rouholahnejad Freund, E., Treydte, K., Schaub, M., Haeni, M., Weiler,  
1018 M., Seeger, S., Marshall, J., Hug, C., Zweifel, R., Hagedorn, F., Rigling, A., Saurer, M., &  
1019 Meusburger, K. (2022). Drought reduces water uptake in beech from the drying topsoil, but  
1020 no compensatory uptake occurs from deeper soil layers. *New Phytologist*, 233(1), 194–206.  
1021 <https://doi.org/10.1111/nph.17767>
- 1022 Gómez-Navarro, C., Pataki, D. E., Bowen, G. J., & Oerter, E. J. (2019). Spatiotemporal  
1023 variability in water sources of urban soils and trees in the semiarid, irrigated Salt Lake  
1024 Valley. *Ecohydrology*, 12(8). <https://doi.org/10.1002/eco.2154>
- 1025 Gonfiantini, R., Wassenaar, L. I., Araguas-Araguas, L., & Aggarwal, P. K. (2018). A unified  
1026 Craig-Gordon isotope model of stable hydrogen and oxygen isotope fractionation during  
1027 fresh or saltwater evaporation. *Geochimica et Cosmochimica Acta*, 235, 224–236.  
1028 <https://doi.org/10.1016/j.gca.2018.05.020>
- 1029 Good, S. P., Noone, D., & Bowen, G. J. (2015). Hydrologic connectivity constrains partitioning  
1030 of global terrestrial water fluxes. *Science*, 349(6244), 175–177.  
1031 <https://doi.org/10.1126/science.aaa5931>

1032 Green, M. B., Laursen, B. K., Campbell, J. L., Mcguire, K. J., & Kelsey, E. P. (2015). Stable  
1033 water isotopes suggest sub-canopy water recycling in a northern forested catchment.  
1034 *Hydrological Processes*, 29(25), 5193–5202. <https://doi.org/10.1002/hyp.10706>

1035 Groh, J., Stumpp, C., Lücke, A., Pütz, T., Vanderborght, J. and Vereecken, H., (2018), Inverse  
1036 estimation of soil hydraulic and transport parameters of layered soils from water stable  
1037 isotope and lysimeter data. *Vadose Zone Journal*, 17(1), pp.1-19.

1038 Gupta, P., Noone, D., Galewsky, J., Sweeney, C., and Vaughn, B.H. (2009) Demonstration of  
1039 high-precision continuous measurements of water vapor isotopologues in laboratory and  
1040 remote field deployments using wavelength-scanned cavity ring-down spectroscopy (WS-  
1041 CRDS) technology. *Rapid Com. in Mass Spectrometry Volume 23, Issue 16, Date: 30*  
1042 *August 2009, Pages: 2534-2542*

1043 Harms Sarah M, & Ludwig, T. K. (2016). Retention and removal of nitrogen and phosphorus in  
1044 saturated soils of arctic hillslopes. *Biogeochemistry*, 127, 291–304.  
1045 <https://doi.org/10.1007/s10533-016-0181-0>

1046 Havranek, R. E., Snell, K. E., Davidheiser-Kroll, B., Bowen, G. J., & Vaughn, B. (2020). The  
1047 Soil Water Isotope Storage System (SWISS): An integrated soil water vapor sampling and  
1048 multiport storage system for stable isotope geochemistry. *Rapid Communications in Mass*  
1049 *Spectrometry*, 34(12), 1–11. <https://doi.org/10.1002/rcm.8783>

1050 Hinckley, E.-L. S., Barnes, R. T., Anderson, S. P., Williams, M. W., & Bernasconi, S. M. (2014).  
1051 Nitrogen retention and transport differ by hillslope aspect at the rain-snow transition of the  
1052 Colorado Front Range. *Journal of Geophysical Research: Biogeosciences*, 119, 12811896.  
1053 <https://doi.org/10.1002/2013JG002588>

1054 Kübert, A., Paulus, S., Dahlmann, A., Werner, C., Rothfuss, Y., Orłowski, N., & Dubbertm  
1055 Maren. (2020). Water Stable Isotopes in Ecohydrological Field Research : Comparison  
1056 Between In Situ and Destructive Monitoring Methods to Determine Soil Water Isotopic  
1057 Signatures. *Frontiers in Plant Science*, 11(April), 1–13.  
1058 <https://doi.org/10.3389/fpls.2020.00387>

1059 Kühnhammer, K., Dahlmann, A., Iraheta, A., Gerchow, M., Birkel, C., Marshall, J. D., & Beyer,  
1060 M. (2022). Continuous in situ measurements of water stable isotopes in soils, tree trunk and  
1061 root xylem: Field approval. *Rapid Communications in Mass Spectrometry*, 36(5).  
1062 <https://doi.org/10.1002/rcm.9232>

1063 Magh, R.K., Gralher, B., Herbstritt, B., Kübert, A., Lim, H., Lundmark, T. and Marshall, J.,  
1064 2022. Conservative storage of water vapour—practical in situ sampling of stable isotopes in  
1065 tree stems. *Hydrology and Earth System Sciences*, 26(13), pp.3573-3587.

1066 Mahindawansa, A., Orłowski, N., Kraft, P., Rothfuss, Y., Racela, H., & Breuer, L. (2018).  
1067 Quantification of plant water uptake by water stable isotopes in rice paddy systems. *Plant*  
1068 *and Soil*, 429(1–2), 281–302. <https://doi.org/10.1007/s11104-018-3693-7>

1069 Oerter, E. J., Perelet, A., Pardyjak, E., & Bowen, G. J. (2016). Membrane inlet laser  
1070 spectroscopy to measure H and O stable isotope compositions of soil and sediment pore  
1071 water with high sample throughput. *Rapid Communications in Mass Spectrometry*, 31(1),  
1072 75–84. <https://doi.org/10.1002/rcm.7768>

- 1073 Oerter, E. J., & Bowen, G. J. (2017). In situ monitoring of H and O stable isotopes in soil water  
 1074 reveals ecohydrologic dynamics in managed soil systems. *Ecohydrology*, *10*(4), 1–13.  
 1075 <https://doi.org/10.1002/eco.1841>
- 1076 Oerter, E. J., & Bowen, G. J. (2019). Spatio-temporal heterogeneity in soil water stable isotopic  
 1077 composition and its ecohydrologic implications in semiarid ecosystems. *Hydrological*  
 1078 *Processes*, *March*, 1–15. <https://doi.org/10.1002/hyp.13434>
- 1079 Peterson, B. J., & Fry, B. (1987). Stable Isotopes in Ecosystem Studies. *Annual Reviews of*  
 1080 *Ecology and Systematics*, *18*, 293–320. <http://www.jstor.org/stable/2097134>
- 1081 Quade, M., Klosterhalfen, A., Graf, A., Brüggemann, N., Hermes, N., Vereecken, H., &  
 1082 Rothfuss, Y. (2019). In-situ monitoring of soil water isotopic composition for partitioning of  
 1083 evapotranspiration during one growing season of sugar beet (*Beta vulgaris*). *Agricultural*  
 1084 *and Forest Meteorology*, *266–267*(December 2018), 53–64.  
 1085 <https://doi.org/10.1016/j.agrformet.2018.12.002>
- 1086 Quade, M., Brüggemann, N., Graf, A., Vanderborght, J., Vereecken, H., & Rothfuss, Y. (2018).  
 1087 Investigation of Kinetic Isotopic Fractionation of Water during Bare Soil Evaporation.  
 1088 *Water Resources Research*, *54*(9), 6909–6928. <https://doi.org/10.1029/2018WR023159>
- 1089 Rothfuss, Y., Vereecken, H., & Brüggemann, N. (2013). Monitoring water stable isotopic  
 1090 composition in soils using gas-permeable tubing and infrared laser absorption spectroscopy.  
 1091 *Water Resources Research*. <https://doi.org/10.1002/wrcr.20311>
- 1092 Rothfuss, Y., Merz, S., Vanderborght, J., Hermes, N., Weuthen, A., Pohlmeier, A., Vereecken,  
 1093 H., & Brüggemann, N. (2015). Long-term and high-frequency non-destructive monitoring  
 1094 of water stable isotope profiles in an evaporating soil column. *Hydrology and Earth System*  
 1095 *Sciences*, *19*(10), 4067–4080. <https://doi.org/10.5194/hess-19-4067-2015>
- 1096 Rothfuss, Y., Quade, M., Brüggemann, N., Graf, A., Vereecken, H., & Dubbert, M. (2021).  
 1097 Reviews and syntheses: Gaining insights into evapotranspiration partitioning with novel  
 1098 isotopic monitoring methods. In *Biogeosciences* (Vol. 18, Issue 12, pp. 3701–3732).  
 1099 Copernicus GmbH. <https://doi.org/10.5194/bg-18-3701-2021>
- 1100 Rozmiarek, K. S., Vaughn, B. H., Jones, T. R., Morris, V., Skorski, W. B., Hughes, A. G.,  
 1101 Elston, J., Wahl, S., Faber, A. K., & Steen-Larsen, H. C. (2021). An unmanned aerial  
 1102 vehicle sampling platform for atmospheric water vapor isotopes in polar environments.  
 1103 *Atmospheric Measurement Techniques*, *14*(11), 7045–7067. [https://doi.org/10.5194/amt-14-](https://doi.org/10.5194/amt-14-7045-2021)  
 1104 [7045-2021](https://doi.org/10.5194/amt-14-7045-2021)
- 1105 Seeger, S., & Weiler, M. (2021). Temporal dynamics of tree xylem water isotopes: In situ  
 1106 monitoring and modeling. *Biogeosciences*, *18*(15), 4603–4627. [https://doi.org/10.5194/bg-](https://doi.org/10.5194/bg-18-4603-2021)  
 1107 [18-4603-2021](https://doi.org/10.5194/bg-18-4603-2021)
- 1108 Soderberg, K., Good, S. P., Wang, L., & Caylor, K. (2012). Stable Isotopes of Water Vapor in  
 1109 the Vadose Zone: A Review of Measurement and Modeling Techniques. *Vadose Zone*  
 1110 *Journal*, *11*(3), 0. <https://doi.org/10.2136/vzj2011.0165>
- 1111 Soil Survey Staff, Natural Resources Conservation Service, United States Department of  
 1112 Agriculture. Soil Series Classification Database. Available online. Accessed 09/10/2022.

- 1113 Sprenger, M., Leistert, H., Gimbei, G., & Weiler, M. (2016). Illuminating hydrological processes  
 1114 at the soil-vegetation-atmosphere interface with water stable isotopes. *Reviews in*  
 1115 *Geophysics*, 54, 674–704. <https://doi.org/10.1002/2015RG000515>
- 1116 Sprenger, M., & Allen, S. T. (2020). What Ecohydrologic Separation Is and Where We Can Go  
 1117 With It. In *Water Resources Research* (Vol. 56, Issue 7). Blackwell Publishing Ltd.  
 1118 <https://doi.org/10.1029/2020WR027238>
- 1119 Stumpp, C., Stichler, W., Kandolf, M. and Šimůnek, J., (2012). Effects of land cover and  
 1120 fertilization method on water flow and solute transport in five lysimeters: A long-term study  
 1121 using stable water isotopes. *Vadose Zone Journal*, 11(1).
- 1122 Theis, D. E., Saurer, M., Blum, H., Frossard, E., & Siegwolf, R. T. W. (2004). A portable  
 1123 automated system for trace gas sampling in the field and stable isotope analysis in the  
 1124 laboratory. *Rapid Communications in Mass Spectrometry*, 18(18), 2106–2112.  
 1125 <https://doi.org/10.1002/rcm.1596>
- 1126 Vereecken, H., Amelung, W., Bauke, S. L., Bogaen, H., Brüggemann, N., Montzka, C.,  
 1127 Vanderborght, J., Bechtold, M., Blöschl, G., Carminati, A., Javaux, M., Konings, A. G.,  
 1128 Kusche, J., Neuweiler, I., Or, D., Steele-Dunne, S., Verhoef, A., Young, M., & Zhang, Y.  
 1129 (2022). Soil hydrology in the Earth system. *Nature Reviews Earth & Environment*.  
 1130 <https://doi.org/10.1038/s43017-022-00324-6>
- 1131 Volkmann, T. H. M., & Weiler, M. (2014). Continual in situ monitoring of pore water stable  
 1132 isotopes in the subsurface. *Hydrology and Earth System Sciences*, 18(5), 1819–1833.  
 1133 <https://doi.org/10.5194/hess-18-1819-2014>
- 1134 Volkmann, T. H. M., Haberer, K., Gessler, A., & Weiler, M. (2016). High-resolution isotope  
 1135 measurements resolve rapid ecohydrological dynamics at the soil-plant interface. *New*  
 1136 *Phytologist*, 210(3), 839–849. <https://doi.org/10.1111/nph.13868>
- 1137 Wassenaar, L. I., Hendry, M. J., Chostner, V. L., & Lis, G. P. (2008). High resolution pore water  
 1138  $\delta^2\text{H}$  and  $\delta^{18}\text{O}$  measurements by  $\text{H}_2\text{O}(\text{liquid})\text{-H}_2\text{O}(\text{vapor})$  equilibration laser  
 1139 spectroscopy. *Environmental Science and Technology*, 42(24), 9262–9267.  
 1140 <https://doi.org/10.1021/es802065s>
- 1141 Zhao, P., Tang, X., Zhao, P., Wang, C. and Tang, J., 2013. Identifying the water source for  
 1142 subsurface flow with deuterium and oxygen-18 isotopes of soil water collected from tension  
 1143 lysimeters and cores. *Journal of Hydrology*, 503, pp.1-10
- 1144 Zimmermann, U., Munnich, K. O., & Roether, W. (1966). Tracers Determine Movement of Soil  
 1145 Moisture and Evapotranspiration. *Science*, 152(3720), 346–347.  
 1146 <https://doi.org/10.1126/science.152.3720.346>